EVALUATION OF NEW PROBES AND APPROACHES FOR CORRELATING OPTICAL AND NUCLEAR IMAGING: APPLICATIONS IN CANCER DETECTION AND TREATMENT

By LAURA BANEVICIUS, B.Sc.

A Thesis Submitted to the Department of Medical Physics & Applied Radiation Sciences and the School of Graduate Studies of McMaster University in Partial Fulfilment of the Requirements for Degree of Master of Science

Master of Science (2013) McMaster University

(Medical Physics) Hamilton, Ontario, Canada

TITLE: Evaluation of New Probes and Approaches for Correlating Optical and Nuclear Imaging: Applications in Cancer Detection and Treatment

AUTHOR: Laura Banevicius

B.Sc., (Medical Physics)

McMaster University, Hamilton, ON, Canada

SUPERVISOR: Dr. John Valliant

NUMBER OF PAGES: viii, 108

Abstract

The photophysical and biological properties of a series of novel molecules that can be used for dual-purpose molecular imaging (optical and nuclear) and therapy of cancer were evaluated. Specifically isostructural [2+1] Re/Tc complexes, a porphyrin conjugate and an antibody-recruiting small molecule construct capable of targeting prostate specific membrane antigen (PSMA) were assessed.

The isostructural [2+1] metal complexes were synthesized to act as an optical probe when prepared using rhenium and a nuclear probe for SPECT when the core metal is ^{99m}Tc. The rhenium analogues were incubated with MCF-7 cells and confocal imaging was used to visualize the uptake of a rhenium bipyridine cyclohexyl nicotinate derivative. Uptake of the ^{99m}Tc complexes in MCF-7 cells were also measured and showed approximately 7% uptake for the pyridine methanol derivative and 5% for the cyclohexyl nicotinate derivative at 120 min. These results demonstrated the utility of the [2+1] isostructural compounds to create dual purpose optical/nuclear imaging agents.

As a complementary approach to the [2+1] complexes, a series of targeted porphyrin derivatives were prepared and screened in vitro. A set of PSMA targeted chlorin e6 (Ce6) derivatives which act as isostructural molecular imaging probes and targeted photosensitizers for photodynamic therapy (PDT) were evaluated. Ce6 was linked to a potent glutamate-urea-lysine based inhibitor of prostate specific membrane antigen (PSMA), which is a transmembrane protein overexpressed in malignant prostate cancer.

Studies in PSMA positive LNCaP cells showed greater uptake of the agents compared to cells with minimal PSMA expression.

Building on the chlorin PSMA studies, a set of antibody-recruiting small molecules that target prostate cancer, and also act as a SPECT imaging agent (when radiolabeled with ^{123}I) or a radiotherapeutic (when labelled with ^{131}I) were developed. These small molecules consist of a PSMA-inhibitor on one end and 2,4-dinitrophenyl (DNP) group on the other which recruits anti-DNP antibodies. A plate reader assay was developed using a PSMA-positive cell line and fluorescently labeled anti-DNP to observe binding and recruitment of antibodies through fluorescence. An iodine-containing derivative with a PEG_8 chain between the PSMA inhibitor and DNP was found to be potent (IC_{50} = 14 nM) and is therefore an attractive candidate for combined radio- and antibody recruiting therapy.

Acknowledgments

First and foremost I would like to thank my supervisor Dr. John Valliant for his insight, guidance and help he has given me. I am grateful for the continued support and collaboration with the many graduate students, post docs and collaborators in the Valliant research group that I have had the privilege of working beside. I would especially like to thank Dr. Afaf Genady and Dr. Selvi Pitchumony for the synthesis of the compounds for use in my project. I want to express my gratitude to my committee members Professors Nicholas Bock and Michael Patterson, for their insight and comments on my work. Furthermore, I would also like to thank the CPDC biology team (Shannon Czorny, Megan Blacker and Nancy Janzen) for their guidance and support. My education as a whole would of course not have been possible without the continued moral support of my friends and family.

Contents

List of Figures and Tables

List of Abbreviations

ABT	antibody terminus
As-Cs	acetylated-chondroitin sulfate
ARM	antibody-recruiting molecule
ATCC	American type culture collection
BODIPY	boron dipyrromethene
BSA	bovine serum albumin
CBT	cell binding terminus
CCCP	carbonylcyanide-m-chlorophenylhydrazone
CCD	charge-coupled device
Ce6	chlorin e6
CHN	cyclohexyl nicotinate
CPM	counts per minute
CT	computed tomography
CTX	chlorotoxin
DCE	dynamic contrast enhanced
DCFBC	N-[N-[(S)-1,3-dicarboxypropyl]carbamoyl]-4-fluorobenzyl-L-cysteine
DMAP	4-dimethylaminopyridine
DMEM	Dulbecco's modified eagle medium
DMSO	dimethyl sulfoxide
DNP	2,4-dinitrophenyl
DOTA	1,4,7,10-tetraazacyclododecane-1,4,7,10-tetraacetic acid

DRE	digital rectal examination
EGFR	epidermal growth factor receptor
EPR	enhanced permeability and retention
FDG	fluorodeoxyglucose
fMRI	functional magnetic resonance imaging
FMT	fluorescence-mediated tomography
FPR	formyl peptide receptor
FRI	fluorescence reflectance imaging
HEPES	4-(2-hydroxyethyl)-1-piperazineethanesulfonic acid
HPLC	high performance liquid chromatography
HRMS	high resolution mass spectra
IC_{50}	half maximal inhibitory concentration
ICG	indocyanine green
IgG	immunoglobulin G
IgM	immunoglobulin M
ID/g	injected dose per gram
KLH	keyhole limpet hemocyanin
LDL	low density lipoprotein
LOR	line of response
LRB	lissamine rhodamine B
mAb	monoclonal antibody
MACE	mono-L-aspartyl chlorin e6
MDP	methylene diphosphonate
MTD	maximum tolerated dose

mIBG	metaiodobenzylguanidine
MRI	magnetic resonance imaging
MTS	3-(4,5-dimethylthiazol-2-yl)-5-(3-carboxymethoxyphenyl)-2-(4-sulfophenyl)-2H-tetrazolium
MTT	3-[4,5-dimethylthiazol-2-yl]-2,5 diphenyl tetrazolium bromide
NAALADase	N-acetylated alpha-linked acidic dipeptidase
NAAG	N-acetylaspartylglutamate
NIR	near-infrared
NMR	nuclear magnetic resonance
PBS	phosphate buffered saline
PDD	photodynamic diagnosis
PDT	photodynamic therapy
PEG	polyethylene glycol
PET	positron emission tomography
PFA	paraformaldehyde
PM	3-pyridylmethanol
PMPA	2-(Phosphonomethyl)-pentanedioic acid
PS	photosensitizer
PSA	prostate-specific antigen
PSMA	prostate specific membrane antigen
PVP	polyvinylpyrrolidone
RA	risedronic acid
RIPA	radioimmunoprecipitation assay
ROS	reactive oxygen species

SAAC	single amino acid chelate
SPE	solid-phase extraction
SPECT	single photon emission computed tomography
TAAG	triazole appending agent
TAG-72	tumour-associated glycoprotein 72
TBS	tris-buffered saline
TCO	trans-cyclooctene
TMRE	tetramethylrhodamine
TRUS	transrectal ultrasound
uPA	urokinase-type plasminogen activator
uPAR	urokinase-type plasminogen activator receptor
US	ultrasound

Chapter 1: Introduction

1.1 Synopsis and Objectives

The goal of the work presented was to evaluate new constructs that can be used as isostructural nuclear and optical imaging probes or as isostructural diagnostic – therapeutic agents. The approach taken involved assessing the properties of three different core constructs: 1) New tridentate Tc/Re chelates targeting PSMA 2) Metal binding porphyrins targeting prostate specific membrane antigen (PSMA) and 3) A new class of isostructural [2+1] metal complexes. The analysis of the photophysical and biological properties of these new constructs was conducted, and additionally, the capacity to introduce antibody recruitment therapy to these unique constructs was assessed.

1.2 Overview of Molecular Imaging

Molecular imaging allows for the visualization and characterization of biological processes non- or minimally invasively. Unlike principally conventional anatomical modalities such as x-ray and computed tomography (CT), molecular imaging relies on creating an image based on a specific biological property of the tissue to be imaged. Molecular imaging modalities include positron emission tomography (PET), single photon emission computed tomography (SPECT), magnetic resonance imaging (MRI), and ultrasound (US). Although MRI has superior spatial resolution, nuclear and optical imaging techniques have higher sensitivity. To compare, the amount of a contrast agent

(probe) needed to generate a detectable signal for each modality is: PET - 10^{-11}-10^{-12} mol/L, SPECT - 10^{-10}-10^{-11} mol/L, optical fluorescence imaging – approximately 10^{-9} to 10^{-12} mol/L and MRI - 10^{-3}-10^{-5} mol/L. The larger amount of the agent needed for MRI versus that for PET or SPECT (micrograms to milligrams for MRI, versus nanograms for PET/SPECT), increases the challenge of developing site specific imaging probes for MRI. Radiolabeled and optical imaging agents in contrast can readily be directed to localize to a specific target of interest.[1]

1.2.1 Nuclear Imaging

Nuclear imaging includes both PET and SPECT. Both systems work through detection of emitted gamma rays, and provide high sensitivity and specificity. PET has the advantage of superior spatial resolution of 2-5 mm versus that of SPECT which is in the range of 7.5-10 mm.[2] SPECT however is more easily accessible as there are more SPECT cameras than PET systems and the associated isotopes are generally less expensive and have longer half-lives.[3]

PET involves the emission of a positron by a positron-emitting radioisotope. The subsequent collision with an electron results in an annihilation process, creating two 511 keV gamma rays approximately 180 degrees apart. If detection of these two gamma rays falls within the coincidence time frame, a line connecting the interaction of the photons with the detectors, called a line of response (LOR), is generated and used for image reconstruction.

Common PET radioisotopes include carbon-11, nitrogen-13, oxygen-15, copper-64, fluorine-18, gallium-68, zirconium-89, iodine-124, with ^{11}C and ^{18}F being the most commonly used.[4-6] ^{18}F-fluorodeoxyglucose (FDG) is the most frequently used PET radiopharmaceutical. ^{18}F-FDG works on the principle that tumours have an altered metabolism in comparison to normal tissue.[7] Many tumour cells in this altered metabolic state will internalize greater amounts of glucose due to the larger amount of glucose transport proteins on their surface. ^{18}F-FDG is an analogue of 2-deoxyglucose, and will therefore be taken up and retained more readily in tumours compared to normal tissue.[7]

SPECT involves the detection of gamma rays by a sodium iodide crystal or analogous type of detector. The gamma rays first pass through a collimator, which is a series of lead walls which let through gamma rays coming from certain angles, usually perpendicularly to the patient. Photons absorbed in the sodium iodide crystal emit light, and this light is converted into an electrical signal that is amplified by the photomultiplier tubes (PMTs). The amplitude of the pulse produced by each PMT is proportional to the amount of light received from the gamma-ray interaction within the crystal. The pattern of photon interactions in the crystal forms a 2D projection of the three-dimensional activity distribution. Images taken at different points around the patient are used to produce a reconstructed 3D image.[8]

Common SPECT radioisotopes include technetium-99m, indium-111, iodine-123 and gallium-67.[3,9] SPECT radioisotopes generally have longer half-lives than those used for PET and do not require a cyclotron for production.[10] Technetium-99m is the most commonly used isotope for SPECT. It is relatively low in cost and readily available, and

the 6 hour half life is ideal because it allows for sufficient preparation time and distribution of the radiolabeled molecule in vivo. Additionally, the nuclear properties and short half life minimize the radiation dose to patients.[3]

PET and SPECT nuclear probes can be directed to bind to a particular target associated with disease. Targeted nuclear imaging probes generally consist of a radiolabeled ligand attached to a targeting vector though a linker. The targeting vector directs the probe to the receptor/target of interest (Figure 1).

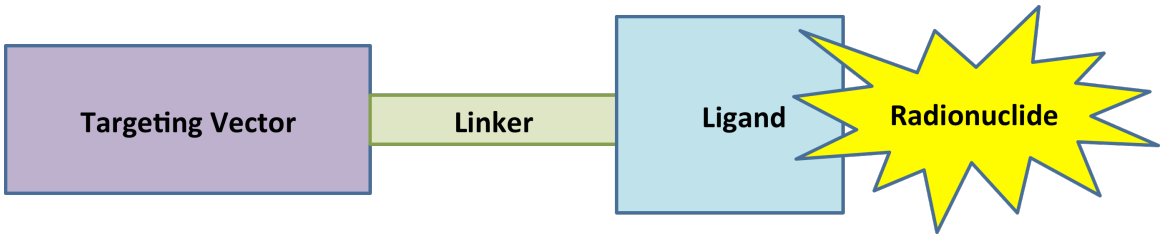

Figure 1: Representative structure of a targeted nuclear imaging probe. A radiolabeled ligand is attached to a targeting vector through a linker group.

The requirements for an effective targeted probe include high binding affinity to the target of interest, stability in blood, good clearance, as well as appropriate contact time and retention with the target in vivo.[11] In order to bind to the receptor of interest, the appropriate choice of targeting vector is needed. To achieve these features a targeting vector that has high affinity for the site of interest is selected, and labelled with a suitable isotope containing ligand or prosthetic group. The construct must maintain its binding affinity when conjugated to the appropriate signalling agent.[12]

Antibodies and small molecules are the two most prevalent methods for targeting a specific receptor associated with cancer, and both have their advantages and disadvantages. Antibodies typically have high specificity and affinity for the target of interest, and are typically stable in blood. They also generally retain their binding affinity when conjugated with the signalling agent. In addition, antibodies have the advantage that they can induce an immune response against the tumour once bound to the target. The pharmokinetic properties of antibodies however are non-ideal, requiring days between injection and imaging. In contrast, small molecules are advantageous as targeting agents due to their fast blood clearance and targeting, but unlike antibodies they are often impacted negatively by the addition of a signalling group.[12,13]

1.2.2 Optical Imaging

Fluorescence imaging is another sensitive molecular imaging technique, and is commonly used to visualize endogenous fluorescent molecules or to assess the location of a molecular probe in vivo or in vitro. In fluorescence imaging, a fluorophore is excited by a light source, and upon returning to the ground state, light of a longer wavelength is emitted.[14] Each fluorophore has a unique peak excitation and peak emission wavelength, which can be used to visualize select molecules and processes.

For in vivo fluorescence imaging, an ideal optical imaging probe has a peak fluorescence emission as close to the infrared region as possible.[15] This is a consequence of the fact that shorter wavelengths are susceptible to increased Rayleigh scattering, which is

inversely proportional to the fourth power of the wavelength.[16] In addition, another reason for requiring the wavelength be closer to the near-IR is because of autofluorescence. Autofluorescence from the cells is highest in the UV and visible region. There is an ideal 'optical window' in the near-IR region where there is minimal autofluorescence from the cells and absorption by hemoglobin, but the wavelength is not too large that absorption by water occurs.[15,17] Near-infrared fluorescence imaging takes into consideration the need for a longer emission wavelength from the fluorophore, and uses fluorophores with emission wavelengths between 700 and 900 nm.[18]

Two fluorescence imaging techniques commonly used in vivo are NIR fluorescence reflectance imaging (FRI) and fluorescence-mediated tomography (FMT). FRI is a technique performed on tumours near the surface, as the depth of penetration is limited to less than one centimeter.[19] A light source, commonly a laser, is directed towards the region of interest, and a lens system is used to spread the light over a larger area. After excitation of the fluorescent molecules, the fluorescence emissions pass through a filter system and a CCD camera is used for detection.[20] FMT enables visualization of fluorescent probes at depths up to a few centimeters, with a theoretical penetration of 7-14 cm.[14,20] This tomographic approach illuminates the tissue at multiple projections and reconstructs the data to form 3D images of the fluorophore distribution.[20]

FRI can also be applied intraoperatively in order to better delineate tumour margins. A critical complication in the resection of tumours is margin determination. Tumour margins need to be correctly determined in order to spare healthy tissue, blood vessels, and nerves, and to ensure that all cancer cells have been removed. The need to improve

margin determination technology is evident, in that approximately 20-25% of breast cancer patients have tumours that are not removed entirely, and 12-28% of patients have a recurrence in the same location as the initial surgery. Additionally, 20,000-600,000 patients yearly in the US suffer from nerve damage as a result of surgery, indicating that more precision is needed.[21]

Delineation of tumor margins is traditionally determined by a change in colour, vascularity or texture. In order to improve tumour resection and margin delineation, fluorescence methods can be applied. For example, Veiseh *et al*. have developed a 'tumour paint' for delineating glioma tumour margins. The NIR Cy5.5 dye was attached to chlorotoxin (CTX), a peptide that preferentially binds to glioma cells. Biophotonic images were taken of mice containing xenografts for which CTX binds. Specificity was shown by blocking with unlabeled CTX, and pathology was used to validate the fluorescence imaging results. Results indicated exceptional resolution of cancerous and non-cancerous tissue.[22]

Additionally, indocyanine green (ICG) is a clinically approved NIR fluorochrome, and has a peak emission of around 820 nm. Although this dye is non-targeted, it can be taken up in tumours, particularly hepatobiliary cancers. It has also been shown to be taken up preferentially in breast cancer as a result of the enhanced permeability and retention (EPR) effect.[23] Tobis *et al.* demonstrated how the da Vinci Surgical System could be used for fluorescence imaging of ICG for the subsequent removal of renal tumours. This system allows for a surgeon to perform robotic assisted laparoscopy and NIR imaging simultaneously. In one recent study injection of ICG and the subsequent NIR imaging

allowed surgeons to distinguish between renal cortical tumours and normal renal tissue, and pathological validation confirmed that tumour margins were correctly identified.[24]

1.2.3 Multi-Modal Imaging

Multi-modality imaging combines data from two or more distinct imaging systems, thereby producing a combined image repository that enables one to take the advantage of each individual technique. For example, both functional and anatomical information can be obtained by having combined PET/CT and PET/MR systems. While structural images are needed to identify the exact position of a tumour, functional images provide information such as aggressiveness, receptor expression levels or response to targeted therapies. PET/CT is commonly used in the clinic and has an advantage in that the CT scan can be used for attenuation correction, which reduces the scan time as no additional transmission scan needs to be performed with the PET system. However, CT has the disadvantage of increasing the radiation dose to the patient, and it does not have the levels of soft tissue contrast provided by MR.[25,26]

A PET/MR system has been developed more recently, allowing for the greater soft tissue contrast of MR to be utilized in this dual modality approach. MR protocols such as dynamic contrast enhanced imaging (DCE), diffusion imaging and functional MRI (fMRI) can now be incorporated with this system to obtain both anatomical and functional information from the MR system combined with the functional/physiological information provided from PET.[27] Additionally, SPECT/MR systems are being

developed, however progress is behind that of PET/MR. Tsui *et al.* have developed a SPECT insert to fit inside an MR system for small animal imaging.[28]

1.2.4 Dual-Purpose Optical and Nuclear Imaging

An additional combined imaging approach involves probes that serve as both optical and nuclear imaging agents. The nuclear portion of this probe could be used to localize the disease, and the optical portion of the probe could be used for margin determination during surgery or biopsy, or for pathological validation of biopsied tissue.[29] This approach combines the advantages of each individual system. The nuclear portion of the probe can be used for quantitative purposes, which is a weakness of fluorescence in vivo imaging. An optical probe has a further advantage of possible increased specificity if designed to turn on the fluorescent signal only when bound to the target of interest. Another advantage of fluorescence imaging is that each molecule can potentially be excited multiple times further enhancing the theoretical sensitivity. Conversely, once a radionuclide decays it cannot "re-emit". Additionally, a further advantage of a combined system is that optical imaging can also be used to validate the specificity of nuclear probes using high resolution fluorescence microscopy or flow cytometry.[30]

Three general approaches have been taken to create dual purpose optical/nuclear imaging agents. One option is to adapt a nuclear probe by replacing the radionuclide prosthetic group with a fluorophore.[31,32] A second approach is to create radiolabeled analogues of known fluorophores, for example, ^{18}F labeled BODIPY.[33] In our approach, a nuclear

probe initially labeled with technetium-99m may obtain fluorescent properties when labeled with rhenium. Re and ^{99m}Tc complexes have nearly identical structures due to the lanthanide contraction, creating a complementary class of probes. Additionally, when labelled with radioactive rhenium (rhenium-188 or rhenium-186), the probe could be used for targeted radionuclide therapy.

1.3 Cancer Therapy

While molecular imaging probes can be used to identify and characterize tumours, they can also be adapted to introduce therapeutic strategies. A nuclear probe can be labelled with an alpha, beta or suitable gamma emitting radionuclide in place of the PET and SPECT isotope and be used for targeted radionuclide therapy. Additionally, the inherent optical properties of a probe may allow for photodynamic therapy to be employed, where light is used to induce the formation of reactive cancer killing radicals. Lastly, a probe may be adapted to elicit an immune response given that this occurs at concentrations similar to that used to generate nuclear and optical images.

1.3.1 Radiotherapy

Radiation therapy involves the use of ionizing radiation on cancer cells to induce a cytotoxic effect. Targeted radiotherapy allows for the delivery of a lethal dose of ionizing radiation to the tumour site, while minimizing the effect on surrounding regions or organs.[34] Radionuclides that can be used for such an application include the β-emitters

rhenium-188, rhenium-186 and iodine-131. Rhenium-186 is a medium range beta particle emitter, whereas rhenium-188 is a long range beta emitter.[34] Rhenium-186 has an average beta energy of 362 keV and a mean range of 1800 μm, and rhenium-188 has an average beta energy of 764 keV and mean range of 3500 μm.[34,35] Iodine-131 emits low energy beta particles (average energy of 134 keV) that have mean range in soft tissue of 400 μm.[36,37]

Iodine-131 is used clinically to treat such cancers as thyroid and neuroendocrine tumours. ^{131}I therapy is the most common method for treatment of differentiated thyroid cancer, while ^{131}I-metaiodobenzylguanidine (^{131}I-mIBG) targets neuroendrocrine cells as it is structurally similar to norepinephrine. Additionally, ^{131}I-tositumomab (Bexxar) is used for radionuclide therapy for C20 positive non-Hodgkin's lymphoma. Other examples of radionuclide therapy include using lipiodol labelled with ^{131}I or ^{188}Re for hepatocellular carcinomas, and ^{186}Re for treating medium sized arthritic joints (radiosynovectomy).[37]

1.3.2 Photodynamic Therapy

Another form of cancer therapy associated with targeted optical probes involves the use of light as the cancer killing agent. In photodynamic therapy (PDT) a photosensitizer is administered to a patient, and after a given period of time, light of a known wavelength is directed toward the area of interest.[38] This light is absorbed by the photosensitizer, exciting it to the first singlet state. Following intersystem crossing to the first triplet state,

an interaction with oxygen in the cancerous tissue causes the generation of reactive oxygen species (principally singlet oxygen) which are toxic to the cell.[15]

The characteristics of an ideal photosenistizer include low dark toxicity, high singlet oxygen quantum yield, high selectivity of the target, and a long peak absorption wavelength. Prevalent photosensitizers currently used in the clinic include Photofrin, Foscan, Levulan, Visudyne, and Metvix.[39] As an example, Photofrin, a hematoporpyrin derivative, accumulates in rapidly dividing tissue, and is used in the treatment of skin, lung, bladder and esophageal cancers.[40]

Another class of photosensitizers include Chlorin e6 (Ce6). Photolon, or Ce6-PVP, consists of a Ce6 attached to polyvinylpyrrolidone (PVP), and is approved for use as a photosensitizer for skin cancer and mucosal malignancies of hollow organs.[41] Other derivatives of Ce6 that have been explored for photodynamic therapy include mono-$_L$-aspartyl chlorin e6 (MACE), diaspartyl Ce6 and monoseryl Ce6. This class of compounds absorb between 650 and 670 nm, and have in a number of cases been show to have selectivity for tumours.[41]

Selectivity of a photosensitizer is important as to not cause toxicity in healthy tissue. By targeting a photosensitizer to a specific protein over-expressed in cancer, specificity can be improved. Chlorin, for example, has been attached to targeting vectors in order to target receptors over-expressed in cancer such as the folate and insulin receptors. [42,43]

Additionally, many photosensitizers can be used not only for therapy, but also for fluorescence imaging (photodynamic diagnosis – PDD). Upon administration of a

photosensitizer and accumulation in the target of interest, light of the appropriate wavelength for fluorescence and PDT can be directed to the sight of interest to both treat and visualize the tumour.[44] As mentioned previously, these agents and fluorescence imaging can be used for both margin-detection for the resection of cancer, and for monitoring the response to treatment induced by PDT.

As an example, Stefflova *et al.* have demonstrated the use of a NIR fluorescent and photodynamic agent that targets the folate receptor.[45] The photosensitizer, pyropheophorbide (Pyro) was linked to a folate targeting moiety through a peptide sequence in order to deliver the agent to cancer cells that overexpressed the associated receptor.[45] Additionally, Soukos *et al.* assessed the response to treatment of the photosensitizing agent Ce6 linked to an antibody that targeted the epidermal growth factor receptor (EGFR) with an anti-EGFR antibody attached to indocyanine Cy5.5.[46]

1.3.3 Antibody Recruitment Therapy

Small molecule induced immunotherapy is a molecular treatment strategy in which antibody-recruiting molecules (ARMs) are attached to a specific cancer biomarker. The ARM recruits endogenous or exogenous antibodies to the site of interest, thereby inducing an immune response.[47] Spiegel and coworkers have developed antibody recruiting small molecules that target receptors over expressed in a number of cancers including PSMA and urokinase-type plasminogen activator receptor (uPAR), using a 2,4-

dinitrophenyl (DNP) group to induce the immune response. Urokinase-type plasminogen activator (uPA) is a protease involved in tumour metastasis, and binds uPAR. Antibody recruitment for this target was induced using a bifunctional small molecule inhibitor of uPA, which contained DNP at one end. The molecule (ARM-U) bound uPAR, while the DNP induced an immune response by recruiting anti-DNP antibodies.[48] Spiegel and coworkers have also developed antibody recruiting small molecules targeting prostate cancer (ARM-Ps). On one end, the ARM-Ps bind PSMA, which is over expressed in prostate cancer. The other end of the ARM-P contains DNP, which recruits anti-DNP antibodies, subsequently inducing an immune response.[49]

1.4 Targets for Molecular Imaging

Receptors over-expressed or uniquely expressed on tumours allow for probes to be used to differentiate between diseased and normal tissue. The two targets investigated in this thesis are a receptor over expressed in prostate cancer (PSMA) and tumour mitochondria, which have increased membrane potentials in cancer cells.

1.4.1 Prostate Cancer and Prostate Specific Membrane Antigen (PSMA)

Prostate cancer is the most diagnosed cancer in men in Canada, with an expected 23 600 new incidences in 2013.[50] Commonly used methods for detection of prostate cancer include measuring prostate-specific antigen (PSA) levels and digital rectal examinations (DRE). If any of these tests are positive, a transrectal ultrasound (TRUS) guided biopsy

will be performed subsequently.[51,52] Serum PSA levels however often give false positives in approximately 27-56% of cases, resulting in unnecessary biopsies. PSA can be secreted not only in the case of prostate cancer, but in any case that disturbs the prostate and allows leakage of PSA into the microvasculature, such as hyperplasia, prostatitis and infarcts. An additional limitation is that PSA levels cannot predict stage of the cancer or relative agressiveness.[53]

Prostate specific membrane antigen (PSMA) is a type-II transmembrane protein overexpressed in malignant prostate cancer.[54] Although the role of PSMA in the prostate is not known, PSMA has enzymatic activity as NAADLADase and thereby plays a vital role in the central nervous system.[55] NAADLADase hydrolyzes N-acetyl-aspartyl-glutamate (NAAG), thereby releasing glutamate.[56] PSMA is expressed in other tissues such as non-cancerous prostate tissue, the small intestine, the salivary glands, and renal tubular cells, however, levels are approximately 100-1000 fold greater in prostate cancer cells. PSMA expression levels also increase with the stage of the cancer, presence of metastatic disease and in castration-resistant prostate cancer.[57] It has been demonstrated that PSMA is internalized by endocytosis through clathrin-coated pits from the plasma membrane of cells.[58,59]

ProstaScint was the first targeted molecular imaging probe approved for imaging PSMA. Also termed ^{111}In capromab pendetide, this imaging probe consists of a murine monoclonal antibody (7E11-C5.3) attached to a chelator (GYK-DTPA-HCl) which is then radiolabelled with indium-111.[51,60,61] Limitations include the fact that ProstaScint

binds to the internal epitope of PSMA, and can therefore only target non-viable (necrotic) PSMA-expressing cancer cells.[62]

The humanized monoclonal antibody J591 has been shown to target the external domain of PSMA and can be used to image bone metastases resulting from prostate cancer. These antibodies however do not have ideal pharmokinetic properties, as they have slow clearance and recognition of PSMA in vivo.[57] Small molecules have been developed to target PSMA and image prostate cancer. For example, the glutamate-urea-lysine based PSMA inhibitors [^{123}I]MIP-1072 and [^{123}I]MIP-1095 are SPECT imaging agents that have been shown to have high affinity for PSMA. Mice bearing LNCaP (PSMA-positive) xenografts had a 17.3% ID/g in the tumour after 1 hour when injected with [^{123}I]MIP-1072, and when injected with [^{123}I]MIP-1095 had a 34.3% ID/g after 4 hours. SPECT/CT images showed activity in the PC3-PIP tumours (PSMA-positive) and no activity in the PC3-flu (PSMA-negative) tumours for both compounds.[63] A PET equivalent derived from ^{18}F, DCFBC, has also been shown to target PSMA in preclinical and clinical studies.[64,65]

1.4.2 Targeting the Mitochondria

The mitochondria of cancer cells have been shown to have an increased membrane potential in comparison to normal epithelial cells.[66,67] This increased membrane potential in the mitochondria of carcinoma cells can therefore serve as a potential target for cancer. An advantage of targeting the mitochondria is that increased membrane potential is

associated with almost all cancer cells, unlike particular receptors which are present in only some types of cancer.[68] Zhou *et al.* have reported the development of a PET imaging probe, ^{64}Cu(DOTA)(LRB), that targets the increased mitochondrial potential of cancer cells by means of lissamine rhodamine B (LRB). The fluorescent analogue, Cu(DOTA)(LRB), was incubated with both U87MG human glioma cells and normal human fibroblast cells and showed an increased fluorescence signal in the glioma cells.[68] The importance of mitochondrial potential on uptake was also tested through an uncoupling experiment, where CCCP, which causes disruption of the mitochondrial potential in cells, was administered in different concentrations to the U87MG human glioma cells. Fluorescence microscopy was used to show the increased uptake of Cu(DOTA)(LRB) in cells whose mitochondrial potential was not disrupted.[68] Optical imaging of Cu(DOTA)(LRB) was performed in mice bearing U87MG and MDA-MB-435 tumours, and showed good contrast at 4 hours post-injection, indicating it has potential as a dual purpose probe. However, due to tissue attenuation, the contrast could not be quantified.[69]

^{99m}Tc Hexakis 2-methoxyisobutylisonitrile (^{99m}Tc-MIBI or Sestamibi) has been shown to be taken up into the mitochondria of cells in a membrane potential dependant manner.[70,71] Sestamibi is used as a SPECT imaging agent for breast cancer due to the increased mitochondrial membrane potential of cancer cells. A clinical study concluded that a significant difference in uptake of sestamibi was seen for breast cancer and normal breast tissue.[71]

1.5 Thesis Overview

The overall goal is to evaluate constructs to be used as isostructural nuclear/optical imaging agents for cancer, or as therapeutic agents. The photophysical and biological properties of these constructs were assessed for their use as potential imaging probes. To meet these objectives, Chapter 2 describes the evaluation of a set of isostructural [2+1] ligands, while Chapter 3 investigates a porphyrin derivative to be used for optical/nuclear imaging, as well as for photodynamic therapy. The final chapter focuses on combining antibody recruitment and molecular imaging/therapy, and is followed by suggested directions for future research.

1.6 References

1 Massoud, T. F. & Gambhir, S. S. Molecular imaging in living subjects: seeing fundamental biological processes in a new light. *Genes Dev* **17**, 545-580 (2003).

2 Histed, S. N. *et al.* Review of functional/anatomical imaging in oncology. *Nucl Med Commun* **33**, 349-361 (2012).

3 Bartholoma, M., Valliant, J., Maresca, K. P., Babich, J. & Zubieta, J. Single amino acid chelates (SAAC): a strategy for the design of technetium and rhenium radiopharmaceuticals. *Chem Commun* **7**, 493-512 (2009).

4 Schlyer, D. J. PET tracers and radiochemistry. *Ann Acad Med Singapore* **33**, 146-154 (2004).

5 Anderson, C. J. & Ferdani, R. Copper-64 radiopharmaceuticals for PET imaging of cancer: advances in preclinical and clinical research. *Cancer Biother Radiopharm* **24**, 379-393 (2009).

6 Elsinga, P. Present and Future of PET-radiopharmaceuticals. *Nucl Med Rev* **15**, C13-C16 (2012).

7 Shukla, A. K. & Kumar, U. Positron emission tomography: An overview. *J Med Phys* **31**, 13-21 (2006).

8 Bushberg, J. T. *The Essential Physics of Medical Imaging*. (Lippincott Williams & Wilkins, 2002).

9 Frangioni, J. V. New technologies for human cancer imaging. *J Clin Oncol* **26**, 4012-4021 (2008).

10 Wyper, D. J. Functional neuroimaging with single photon emission computed tomography (SPECT). *Cerebrovasc Brain Metab Rev* **5**, 199-217 (1993).

11 Maison, W. & Frangioni, J. V. Improved chemical strategies for the targeted therapy of cancer. *Angew Chem Int Ed Engl* **42**, 4726-4728 (2003).

12 Kuchenthal, C. H. & Maison, W. Antibody recruiting small molecules: a new option for prostate tumor therapy by PSMA targeting. *Chembiochem* **11**, 1052-1054 (2010).

13 Imai, K. & Takaoka, A. Comparing antibody and small-molecule therapies for cancer. *Nat Rev Cancer* **6**, 714-727 (2006).

14 Weissleder, R. & Ntziachristos, V. Shedding light onto live molecular targets. *Nat Med* **9**, 123-128 (2003).

15 Prasad, P. N. *Introduction to Biophotonics*. (Wiley-Interscience, 2003).

16 Niemz, M. H. *Laser-Tissue Interactions: Fundamentals and Applications*. (Springer, 1996).

17 Fujimoto, J. G. & Farkas, D. *Biomedical Optical Imaging*. (Oxford University Press, 2009).

18 Gioux, S., Choi, H. S. & Frangioni, J. V. Image-Guided Surgery Using Invisible Near-Infrared Light: Fundamentals of Clinical Translation. *Mol Imaging* **9**, 237-255 (2010).

19 Weissleder, R. Scaling down imaging: Molecular mapping of cancer in mice. *Nat Rev Cancer* **2**, 11-18 (2002).

20 Ntziachristos, V., Bremer, C. & Weissleder, R. Fluorescence imaging with near-infrared light: new technological advances that enable in vivo molecular imaging. *Eur Radiol* **13**, 195-208 (2003).

21 Gioux, S., Choi, H. S. & Frangioni, J. V. Image-guided surgery using invisible near-infrared light: fundamentals of clinical translation. *Mol Imaging* **9**, 237-255 (2010).

22 Veiseh, M. *et al.* Tumor paint: a chlorotoxin:Cy5.5 bioconjugate for intraoperative visualization of cancer foci. *Cancer Res* **67**, 6882-6888 (2007).

23 Schaafsma, B. E. *et al.* The clinical use of indocyanine green as a near-infrared fluorescent contrast agent for image-guided oncologic surgery. *J Surg Oncol* **104**, 323-332 (2011).

24 Tobis, S. *et al.* Near infrared fluorescence imaging with robotic assisted laparoscopic partial nephrectomy: initial clinical experience for renal cortical tumors. *J Urol* **186**, 47-52 (2011).

25 Bolus, N. E., George, R., Washington, J. & Newcomer, B. R. PET/MRI: the blended-modality choice of the future? *J Nucl Med Technol* **37**, 63-71 (2009).

26 Pichler, B. J., Kolb, A., Nagele, T. & Schlemmer, H. P. PET/MRI: paving the way for the next generation of clinical multimodality imaging applications. *J Nucl Med* **51**, 333-336 (2010).

27 Pichler, B. J., Wehrl, H. F., Kolb, A. & Judenhofer, M. S. Positron Emission Tomography/Magnetic Resonance Imaging: The Next Generation of Multimodality Imaging? *Semin Nucl Med* **38**, 199-208 (2008).

28 Tsui, B. M. W. *et al.* in *2011 Ieee Nuclear Science Symposium and Medical Imaging Conference IEEE Nuclear Science Symposium Conference Record* 3178-3182 (2011).

29 Lee, S. & Chen, X. Dual-modality probes for in vivo molecular imaging. *Mol Imaging* **8**, 87-100 (2009).

30 Culver, J., Akers, W. & Achilefu, S. Multimodality molecular imaging with combined optical and SPECT/PET modalities. *J Nucl Med* **49**, 169-172 (2008).

31 Rao, C. S., Chu, J. J., Liu, R. S. & Lai, Y. K. Synthesis and evaluation of C-14 - labelled and fluorescent-tagged paclitaxel derivatives as new biological probes. *Bioorg Med Chem* **6**, 2193-2204 (1998).

32 Kuil, J., Velders, A. H. & van Leeuwen, F. W. Multimodal tumor-targeting peptides functionalized with both a radio- and a fluorescent label. *Bioconjug Chem* **21**, 1709-1719 (2010).

33 Li, Z. *et al.* Rapid aqueous [18F]-labeling of a bodipy dye for positron emission tomography/fluorescence dual modality imaging. *Chem Commun* **47**, 9324-9326 (2011).

34 Zalutsky, M. R. in *Handbook of Nuclear Chemistry* (Springer, 2011).

35 van der Poel, H. G. Radionuclide Treatment in Metastasized Prostate Cancer. *EAU-EBU Update Series* **5**, 113-125 (2007).

36 Dadachova, E., Bouzahzah, B., Zuckier, L. S. & Pestell, R. G. Rhenium-188 as an alternative to Iodine-131 for treatment of breast tumors expressing the sodium/iodide symporter (NIS). *Nucl Med Biol* **29**, 13-18 (2002).

37 Dash, A., Knapp, F. F. & Pillai, M. R. Targeted Radionuclide Therapy - An Overview. *Curr Radiopharm* **23**, 23 (2013).

38 Celli, J. P. *et al.* Imaging and Photodynamic Therapy: Mechanisms, Monitoring, and Optimization. *Chem Rev.* **110**, 2795-2838 (2010).

39 Huang, Z. A review of progress in clinical photodynamic therapy. *Technol Cancer Res Treat* **4**, 283-293 (2005).

40 Allison, R. R. & Sibata, C. H. Oncologic photodynamic therapy photosensitizers: A clinical review. *Photodiagnosis Photodyn Ther* **7**, 61-75 (2010).

41 Juzeniene, A. Chlorin e6-based photosensitizers for photodynamic therapy and photodiagnosis. *Photodiagnosis Photodyn Ther* **6**, 94-96 (2009).

42 Li, D. *et al.* A novel chlorin-PEG-folate conjugate with higher water solubility, lower cytotoxicity, better tumor targeting and photodynamic activity. *J Photochem Photobiol B* **9**, 28-37 (2013).

43 Akhlynina, T. V., Rosenkranz, A. A., Jans, D. A. & Sobolev, A. S. Insulin-mediated intracellular targeting enhances the photodynamic activity of chlorin e6. *Cancer Res* **55**, 1014-1019 (1995).

44 Celli, J. P. *et al.* Imaging and photodynamic therapy: mechanisms, monitoring, and optimization. *Chem Rev* **110**, 2795-2838 (2010).

45 Stefflova, K., Li, H., Chen, J. & Zheng, G. Peptide-based pharmacomodulation of a cancer-targeted optical imaging and photodynamic therapy agent. *Bioconjug Chem* **18**, 379-388 (2007).

46 Soukos, N. S. *et al.* Epidermal growth factor receptor-targeted immunophotodiagnosis and photoimmunotherapy of oral precancer in vivo. *Cancer Res* **61**, 4490-4496 (2001).

47 Reichert, J. M. & Valge-Archer, V. E. Outlook - Development trends for monoclonal antibody cancer therapeutics. *Nat Rev Drug Discov* **6**, 349-356 (2007).

48 Jakobsche, C. E., McEnaney, P. J., Zhang, A. X. & Spiegel, D. A. Reprogramming urokinase into an antibody-recruiting anticancer agent. *ACS Chem Biol* **7**, 316-321 (2012).

49 Murelli, R. P., Zhang, A. X., Michel, J., Jorgensen, W. L. & Spiegel, D. A. Chemical Control over Immune Recognition: A Class of Antibody-Recruiting Small Molecules That Target Prostate Cancer. *J Am Chem Soc* **131**, 17090-17092 (2009).

50 Canadian Cancer Society's Advisory Committee on Cancer Statistics. Canadian Cancer Statistics 2013. (2013).

51 Manyak, M. J. Indium-111 capromab pendetide in the management of recurrent prostate cancer. *Expert Rev Anticancer Ther* **8**, 175-181 (2008).

52 Penzkofer, T. & Tempany-Afdhal, C. M. Prostate cancer detection and diagnosis: the role of MR and its comparison with other diagnostic modalities - a radiologist's perspective. *NMR Biomed* **3** (2013).

53 Kelloff, G. J., Choyke, P. & Coffey, D. S. Challenges in clinical prostate cancer: role of imaging. *AJR Am J Roentgenol* **192**, 1455-1470 (2009).

54 Chang, S. S. *et al.* Prostate-specific membrane antigen is produced in tumor-associated neovasculature. *Clin Cancer Res* **5**, 2674-2681 (1999).

55 Ghosh, A. & Heston, W. D. W. Tumor target prostate specific membrane antigen (PSMA) and its regulation in prostate cancer. *J Cell Biochem* **91**, 528-539 (2004).

56 Slusher, B. S. *et al.* Selective inhibition of NAALADase, which converts NAAG to glutamate, reduces ischemic brain injury. *Nat Med* **5**, 1396-1402 (1999).

57 Osborne, J. R. *et al.* Prostate-specific membrane antigen-based imaging. *Urol Oncol* **31**, 144-154 (2013).

58 Rajasekaran, A. K., Anilkumar, G. & Christiansen, J. J. Is prostate-specific membrane antigen a multifunctional protein? *Am J Physiol Cell Physiol.* **288**, C975-C981 (2005).

59 Liu, H. *et al.* Constitutive and antibody-induced internalization of prostate-specific membrane antigen. *Cancer Res* **58**, 4055-4060 (1998).

60 Apolo, A. B., Pandit-Taskar, N. & Morris, M. J. Novel Tracers and Their Development for the Imaging of Metastatic Prostate Cancer. *J Nucl Med* **49**, 2031-2041 (2008).

61 Bouchelouche, K., Choyke, P. L. & Capala, J. Prostate Specific Membrane Antigen - A Target for Imaging and Therapy with Radionuclides. *Discov Med* **44**, 55-61 (2010).

62 Vallabhajosula, S., Smith-Jones, P. M., Navarro, V., Goldsmith, S. J. & Bander, N. H. Radioimmunotherapy of prostate cancer in human xenografts using monoclonal antibodies specific to prostate specific membrane antigen (PSMA): studies in nude mice. *Prostate* **58**, 145-155 (2004).

63 Hillier, S. M. *et al.* Preclinical evaluation of novel glutamate-urea-lysine analogues that target prostate-specific membrane antigen as molecular imaging pharmaceuticals for prostate cancer. *Cancer Res* **69**, 6932-6940 (2009).

64 Mease, R. C. *et al.* N-[N-[(S)-1,3-Dicarboxypropyl]carbamoyl]-4-[18F]fluorobenzyl-L-cysteine, [18F]DCFBC: a new imaging probe for prostate cancer. *Clin Cancer Res* **14**, 3036-3043 (2008).

65 Cho, S. Y. *et al.* Biodistribution, tumor detection, and radiation dosimetry of 18F-DCFBC, a low-molecular-weight inhibitor of prostate-specific membrane antigen, in patients with metastatic prostate cancer. *J Nucl Med* **53**, 1883-1891 (2012).

66 Modica-Napolitano, J. S. & Singh, K. K. Mitochondria as targets for detection and treatment of cancer. *Expert Rev Mol Med* **4**, 1-19 (2002).

67 Modicanapolitano, J. S. & Aprille, J. R. Basis for the selective cytotoxicity of rhodamine-123. *Cancer Res* **47**, 4361-4365 (1987).

68 Zhou, Y. *et al.* Cu-64-Labeled Lissamine Rhodamine B: A Promising PET Radiotracer Targeting Tumor Mitochondria. *Mol Pharm* **8**, 1198-1208 (2011).

69 Yan, X., Zhou, Y. & Liu, S. Optical Imaging of Tumors with Copper-Labeled Rhodamine Derivatives by Targeting Mitochondria. *Theranostics* **2**, 988-998 (2012).

70 Piwnica-Worms, D., Kronauge, J. F. & Chiu, M. L. Uptake and retention of hexakis (2-methoxyisobutyl isonitrile) technetium(I) in cultured chick myocardial cells. Mitochondrial and plasma membrane potential dependence. *Circulation* **82**, 1826-1838 (1990).

71 Fleming, R. M. Mitochondrial uptake of sestamibi distinguishes between normal, inflammatory breast changes, pre-cancers, and infiltrating breast cancer. *Integr Cancer Ther* **1**, 229-237 (2002).

Chapter 2: Isostructural 2+1 Ligands

The following chapter presents work on the development and evaluation of isostructural Re/^{99m}Tc nuclear and optical probes. Prior to completing and publishing this work[1] the optical properties of a new chelate known as the single amino acid chelate III (SAACIII) were assessed. After determining the fluorescence emission was too low for further optical studies, the focus shifted to [2+1] Re/^{99m}Tc bipyridine ligands. Section 2.5 is from the published manuscript where my contribution was the imaging and screening of the compounds prepared by Dr. Selvi Pitchumony.

2.1 Introduction

Isostructural Re/Tc complexes can be used to develop optical and nuclear probes from a single construct. When an appropriate ligand is complexed to Re(I) it can be fluorescent and can used as an optical probe, and when complexed to ^{99m}Tc the complex can be used as a nuclear probe for SPECT imaging or quantitative preclinical biodistribution studies. This is the result of the fact that both technetium and rhenium complexes have the same size and comparable chemical properties.

The single amino acid chelate (SAAC) ligand was previously developed by the Valliant group and forms stable complexes with Re(I)/Tc(I).[2] A quinoline analogue (SAACQ) forms a luminescent complex with Re. In vitro fluorescence microscopy studies were performed with

a targeted SAACQ-Re derivative, where the complex was shown to have peak fluorescence emission intensities at 425 and 580 nm. The complex was attached to a targeting vector for the formyl peptide receptor (FPR), which is present on neutrophils, and fluorescence microscopy showed uptake of this complex in human leukocytes.[3]

More recently, the SAAC ligand was adapted to create a more water soluble analogue, the single amino acid chelate III (SAACIII). This new Re/^{99m}Tc chelate developed by the Valliant group was designed to be a nuclear probe for SPECT when complexed to ^{99m}Tc, and an optical probe when complexed to Re (Figure 2). Furthermore, when attached to radioactive rhenium (^{186}Re/^{188}Re), SAACIII can also be used to develop radiotherapy agents. An additional consideration is that SAACIII itself is fluorescent and may be used as an optical probe on its own, even when not complexed to rhenium. SAACIII was successfully attached to a glutamate-urea-lysine derived PSMA inhibitor to target prostate cancer, where its polar nature helped maximize target to non-target ratios.

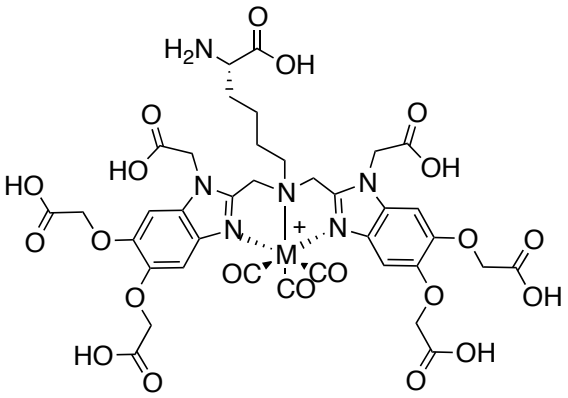

Figure 2: The single amino acid chelate III (SAACIII) can be labelled with either ^{99m}Tc (nuclear) or Re (fluorescent) in order to generate isostructural nuclear and optical probes (M = ^{99m}Tc or Re).

2.2 Goal

While the rhenium and 99m-technetium complexes of SAACIII have been prepared and a PSMA targeted analogue developed, the optical properties of the ligand have not been evaluated. The goal was therefore to assess the optical properties, and if ideal for imaging, proceed to evaluate the construct in vitro. After the validation of adequate optical properties, the optical/nuclear agent could be evaluated for target binding and uptake in the appropriate cell line. The study can eventually be expanded to study uptake and distribution in vivo as well.

2.3 Results

The optical properties of the SAACIII ligand were first assessed where a 40 μM solution of SAACIII in 50% methanol, 50% acetonitrile was measured for absorption and emission with the Tecan Safire plate reader. Peak absorptions were observed to be 258 nm and 295 nm. When excited at each of these peak absorbance wavelengths, the peak emission was 330 nm (Figure 3). Therefore, the ligand itself was found to have a low absorption and emission wavelength making it unsuitable for optical imaging. Additionally, when complexed to Re, the fluorescence was quenched, and fluorescence levels were too low for optical imaging.

Ideally, an optical imaging agent should have an emission wavelength as close to the near-infrared region as possible to minimize scattering and background fluorescence due

to autofluorescence of the cells. Given the observed optical properties the focus of the work shifted.

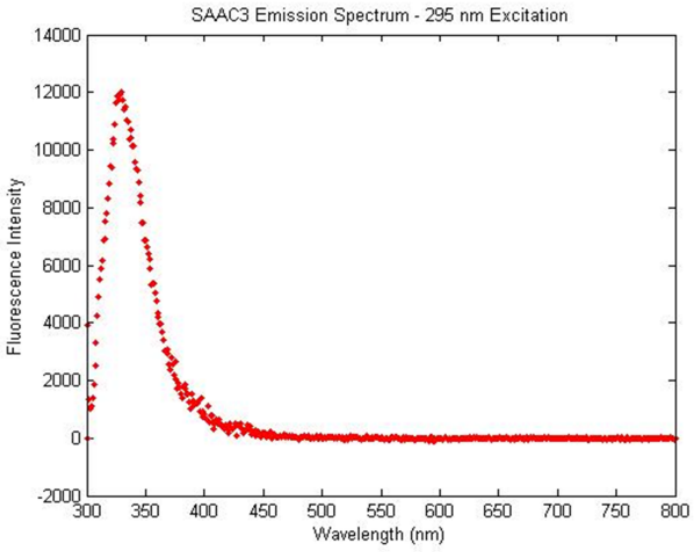

Figure 3: Fluorescence emission spectrum of SAACIII when excited at 295 nm

2.4 New Approach: 2+1 Ligands

Given the limitations of the SAACIII system an alternative class of Re complexes were evaluated. [2+1] Re(I) compounds refer to a class of compounds consisting of a bidentate ("2") ligand (bipyridine) and a monodentate ("1") ligand. The rhenium analogues have been used previously as luminophores including as mitochondrial dyes in MCF-7 cells.[4,5] The Valliant group developed the means to prepare the ^{99m}Tc analogue of these compounds creating a new class of isostructural probes. To demonstrate that they are suitable in this regard it was necessary to assess and compare the uptake of the Re and ^{99m}Tc compounds in vitro.

2.5 Isostructural Nuclear and Luminescent Probes Derived From Stabilized [2+1] Re(I)/Tc(I) Organometallic Complexes

The following sections were published in Inorganic Chemistry[1] where the synthetic work was contributed by Dr. Pitchumony and the preponderance of the biology work completed by myself. The paper describes the synthesis and biological evaluation of a set of [2+1] optical/nuclear bipyridine complexes. My specific contributions include obtaining the fluorescence spectra, cell imaging and the radioactive uptake assays. Specifically, uptake of compounds **2-6** and **2-7** were assessed through confocal microscopy and radioactive uptake in MCF-7 cells. Additionally, a colocalization study was performed to determine if **2-7** localized to the mitochondria. This is presented as a separate section (Section 2.6).

Isostructural Nuclear and Luminescent Probes Derived From Stabilized [2+1] Re(I)/Tc(I) Organometallic Complexes

Tamil Selvi Pitchumony,[a] Laura Banevicius,[b] Nancy Janzen[a], Jon Zubieta,[c] and John F. Valliant[a,d]*

[a]Department of Chemistry and Chemical Biology, McMaster University,

1280 Main St. West, Hamilton ON L8S 4M1, Canada

[b]Department of Medical Physics and Applied Radiation Sciences, McMaster University,

1280 Main St. West, Hamilton ON L8S 4M1, Canada

[c]Department of Chemistry, Syracuse University, Syracuse, NY 13244-4100, USA

[d]Centre for Probe Development and Commercialization, 1280 Main St. West,

Hamilton ON L8S 4M1, Canada

Corresponding Author: John F. Valliant

1280 Main St. W., NRB-A312, McMaster University, Hamilton, ON, L8S 4K1,

Canada

Phone: (905) 525-9140 ext. 20182

Fax: (905) 522-7776

Email: valliant@mcmaster.ca

Abstract

A convenient method to prepare ^{99m}Tc analogues of a class of rhenium(I) fluorophores was developed creating isostructural pairs of nuclear and optical probes. Two step and a new one pot procedures were used to produce a series of [2+1] complexes of the type $[Tc(CO)_3(bipy)L]^+$ in greater than 80% yield. The plasma stability of the reported compounds were evaluated where the basicity of the monodentate pyridine type ligand (L) has a significant impact with half-lives ranging from 2 to 20 hours. The ability to generate the radioactive complexes makes it possible to quantitate cell uptake of Re fluorophores which was demonstrated in MCF-7 breast cancer cells using ^{99m}Tc analogues of two Re(I)-based mitochondrial targeting dyes.

Introduction

The interest in molecular imaging probes that can be used with multiple imaging modalities is being spurred on by the increasing availability of hybrid imaging systems and the enhanced information content that can be derived by employing more than one modality.[6-10] The ability to combine and/or contrast data from complementary imaging technologies creates an opportunity to leverage the strengths and overcome limitations of individual methods. Correlating nuclear and fluorescence imaging for instance makes it possible to relate deep tissue whole-body imaging with histopathology and fluorescence microscopy providing a convenient way to validate the mechanism of binding, selectivity and cellular distribution of targeted radiopharmaceuticals.

To this end molecular imaging probes are being developed whereby targeting vectors are being derivatized with both fluorophore and radionuclide containing prosthetic groups. This way a single construct can be used to generate fluorescent and nuclear (positron emission tomography or single photon emission computed tomography) images. The challenge in developing probes of this type is that the associated prosthetic groups are unto themselves rarely innocent in that they typically have significant impact on the ability of the targeting vector to localize in the desired region/organ *in vivo* and bind to the molecular target of interest. It requires extensive optimization and resources to find the right combination of linker types and sites for derivatization and in many cases the need to add two prosthetic groups limits the type and size of vectors that can be used.

An alternative strategy is to use radiolabeled dyes or chelates which form a luminescent complex with a non-radioactive metal and an isostructural complex with a radioactive isotope of that same element or its congenor (for second and third row transition metals).[11-16] The advantage here is that only one bioconjugate containing a single prosthetic group needs to be developed and optimized to generate both classes of imaging probes. Complexes derived from Re(I)/^{99m}Tc(I) are particularly attractive because of the widespread use, low cost and low dose burden of ^{99m}Tc. Quinoline based ligand systems for instance have been used to prepare luminescent and radioactive Re/Tc probes for a number of applications imaging prostate cancer, infection and for monitoring neurosphere transplants.[3,17-19] Unfortunately, Re complexes of this type posses low quantum yields and their absorbance (peak at 301 nm) and emission (425 and 580 nm)

properties are not ideal for cell and tissue imaging. Furthermore, the ligands generally require heating or long reaction times to form the desired ^{99m}Tc complexes.

Re(I)-tricarbonyl complexes derived from one bidentate polypyridine type donor and one monodentate pyridine type ligand (Figure 4) have been used extensively as ion sensing and cell imaging agents.[20-28] These transition metal luminophores have a number of attractive optical imaging properties but have not been widely investigated as cores for developing radioactive probes because of concerns about premature loss of the monodentate ligand *in vivo* and potential complexities of the radiochemical synthesis, which could hinder clinical translation.[29-31] Our hypothesis was that with the appropriate choice of monodentate ligand and the development of a convenient radiochemical method, compounds of the type $[M(CO)_3(bipy)L]^n$ (where M = Re, ^{99m}Tc, bipy= 2,2'-bipyridine and L=monodentate ligand) could be used to create a new class of isostrucural luminescent and nuclear probes. These complexes should possess desirable optical imaging properties, have low dose consequences when used *in vivo* and would possess the synthetic versatility needed to create structurally and functionally diverse high affinity multi-modal molecular imaging probes.[32-34]

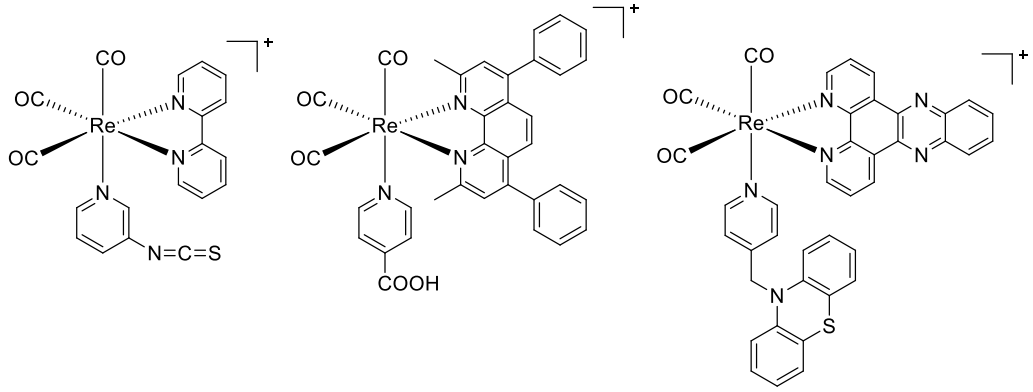

Figure 4: Examples of previously reported [2+1] type luminophores based on pyridine complexes of the $[Re(CO)_3]^+$ core.

Results and Discussion

Radiochemistry

The initial goal was to prepare a series of technetium analogues of $[Re(CO)_3(bipy)(L)]^+$ in which the basicity of the monodentate ligand was varied to assess the overall impact of the complex on stability. Reference standards **2-2**, **2-4a**, **2-5a**, **2-6a** and **2-7a** were prepared following an established methodology in good yields (**Scheme 1**).[4,35] The rhenium complexes were initially synthesized as the triflate salts but were converted to the corresponding chlorides using an ion exchange resin so that they would be identical to the ^{99m}Tc analogues which are prepared in the presence of saline.

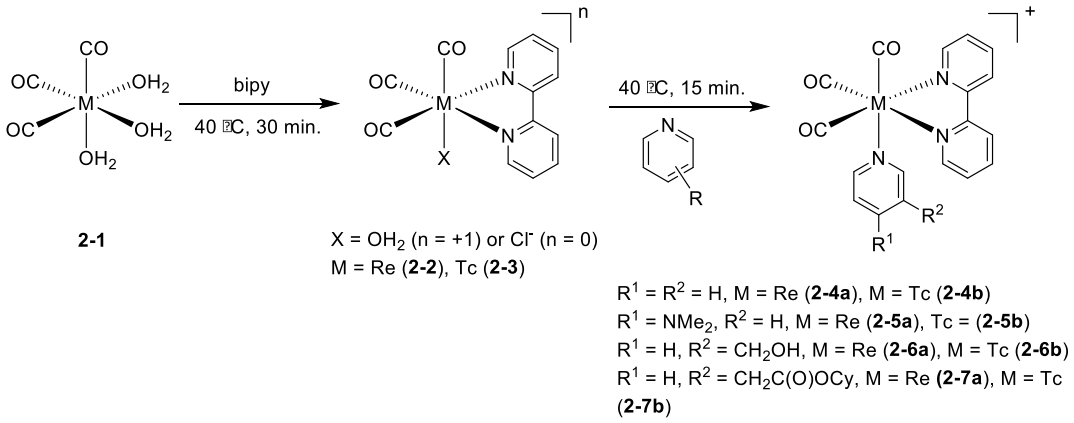

2-1

X = OH_2 (n = +1) or Cl^- (n = 0)
M = Re (**2-2**), Tc (**2-3**)

$R^1 = R^2 = H$, M = Re (**2-4a**), M = Tc (**2-4b**)
$R^1 = NMe_2$, $R^2 = H$, M = Re (**2-5a**), Tc = (**2-5b**)
$R^1 = H$, $R^2 = CH_2OH$, M = Re (**2-6a**), M = Tc (**2-6b**)
$R^1 = H$, $R^2 = CH_2C(O)OCy$, M = Re **(2-7a**), M = Tc (**2-7b**)

Scheme 1. Synthesis of the isostructural [2+1] Re(I) and ^{99m}Tc complexes. Note that the conditions shown are specifically for the reactions run at the tracer level.

The corresponding ^{99m}Tc complexes were synthesised from $[^{99m}Tc(CO)_3(H_2O)_3]^+$ which can be produced in a single step from TcO_4^- following the method developed by Alberto *et al.*[36,37] $[^{99m}Tc(CO)_3(bipy)Cl]$ (**2-3**) was synthesised in high yield by the addition of $[^{99m}Tc(CO)_3(H_2O)_3]^+$ to a vial containing bipyridine and heating the reaction mixture to 40 °C. After 15 min. the reaction was nearly complete showing <10% $[^{99m}Tc(CO)_3(H_2O)_3]^+$ and a single new product formed whose HPLC retention time matched that of $[Re(CO)_3(bipy)Cl]$. Following optimization of pH, temperature and reaction time, quantitative formation of **2-3** can be achieved in 30 min. at 40 °C (Figure 5).

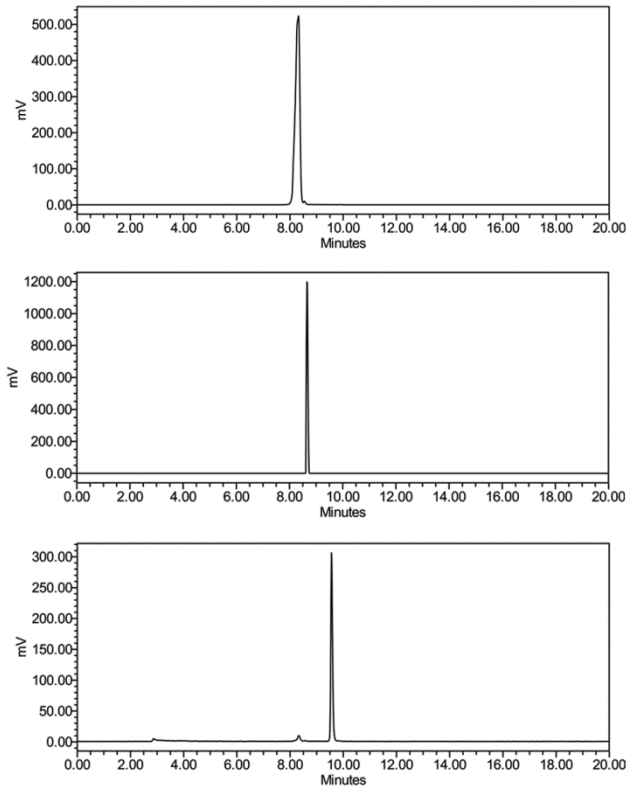

Figure 5: Gamma HPLC traces of $[^{99m}Tc(CO)_3(bipy)Cl]$ (3) (top), $[^{99m}Tc(CO)_3(bipy)(py)]^+$ (2-4b) (middle) and $[^{99m}Tc(CO)_3(bipy)(DMAP)]^+$ (2-5b) (bottom).

The ^{99m}Tc analogue of $[Re(CO)_3(bipy)(py)]^+$ (**2-4a**) was prepared by adding the solution of **2-3** to pyridine and heating for a further 15 min. at 40 °C. The formation of the desired product was achieved in quantitative yield and there was no evidence of residual starting material under these conditions (Figure 5). The product could be readily isolated by solid-phase extraction (SPE) or semi-preparative HPLC free from residual ligand.

These synthesis conditions were equally effective in producing different pyridine derivatives including the 4-dimethylaminopyridine (DMAP, **2-5b**), 3-pyridylmethanol (PM, **2-6b**) and the cyclohexyl nicotinate ester (CHN, **2-7b**) complexes. These ligands were selected as a preliminary assessment of the impact of the basicity of the pyridine ligand on the stability of the complex and because **2-6a** and **2-7a** have been used as cell imaging reagents and were reported to exhibit uptake into specific cellular compartments (*vide infra*).[4]

An attempt was also made to produce a one pot labelling method whereby both the bidentate and monodentate ligands are present in the reaction mixture at the same time. Here the kinetics of the reaction and tendency of the two ligands to coordinate at different pH values was exploited. $[^{99m}Tc(CO)_3(H_2O)_3]^+$ was added to a solution containing bipy and DMAP at pH 2 and the mixture heated to 40 °C. After 15 min. the pH was adjusted to 9 and the reaction allowed to proceed at 40 °C for a further 30 min. yielding the desired product in comparable yield to the two step procedure. HPLC of the reaction mixture at pH 2 and 9 (Figure 6) clearly showed the formation of **2-3** and **2-5b** respectively which was confirmed through comparison of the retention times to that for the corresponding Re standards.

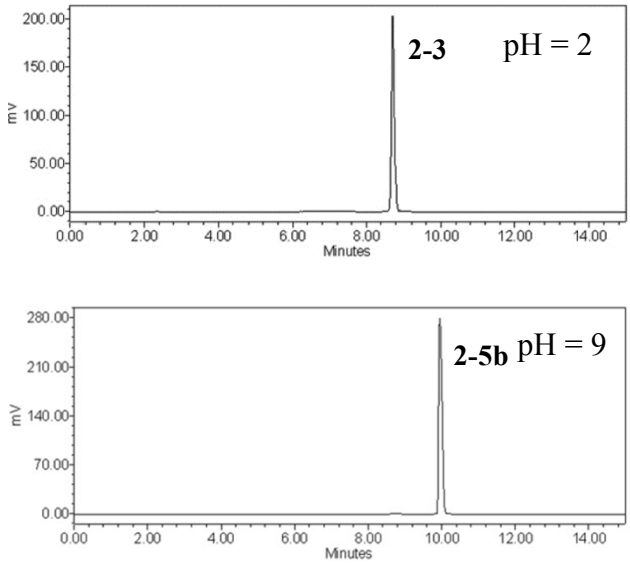

Figure 6: Gamma HPLC traces associated with the one-pot synthesis of $[^{99m}Tc(CO)_3(bipy)(DMAP)]^+$ (2-5b). Gamma HPLC trace of the reaction mixture after 30 min. at pH 2 (top) which shows the formation of $[^{99m}Tc(CO)_3(bipy)Cl]$ (2-3). Gamma HPLC trace (bottom) of the reaction mixture after an additional 15 min. at pH = 9 which shows the formation of 2-5b.

Stability

The stability of the ^{99m}Tc complexes and the extent of protein binding were evaluated in mouse plasma as a function of time (Figure 7). The loss of the monodentate ligand forms a reactive species that exhibits high binding to proteins (>50% in 1 h) through coordination to good donor groups including cysteine and histidine residues; consequently the amount of radioactivity in the plasma along with the associated HPLC analysis, is a good indicator of stability of the complexes *in vitro*. For the pyridine derivative **2-4b**, protein binding at early time points was low; however the time to achieve 50% protein binding was just over two hours. HPLC analysis of the supernatant showed predominately the intact complex even after 3 hours. The pyridylmethanol derivative **2-**

6b showed comparable stability. The more basic DMAP ligand (pKa = 9.2) in contrast, showed low protein binding (<20%) after four hours and only 50% binding at 20 hours. When the Re complexes **2-5a** and **2-6a** were incubated with plasma over six hours, which is longer than what is typically used for cell imaging studies, HPLC analysis following protein precipitation showed almost no loss of product due to protein binding, precipitation or degradation of the complexes.

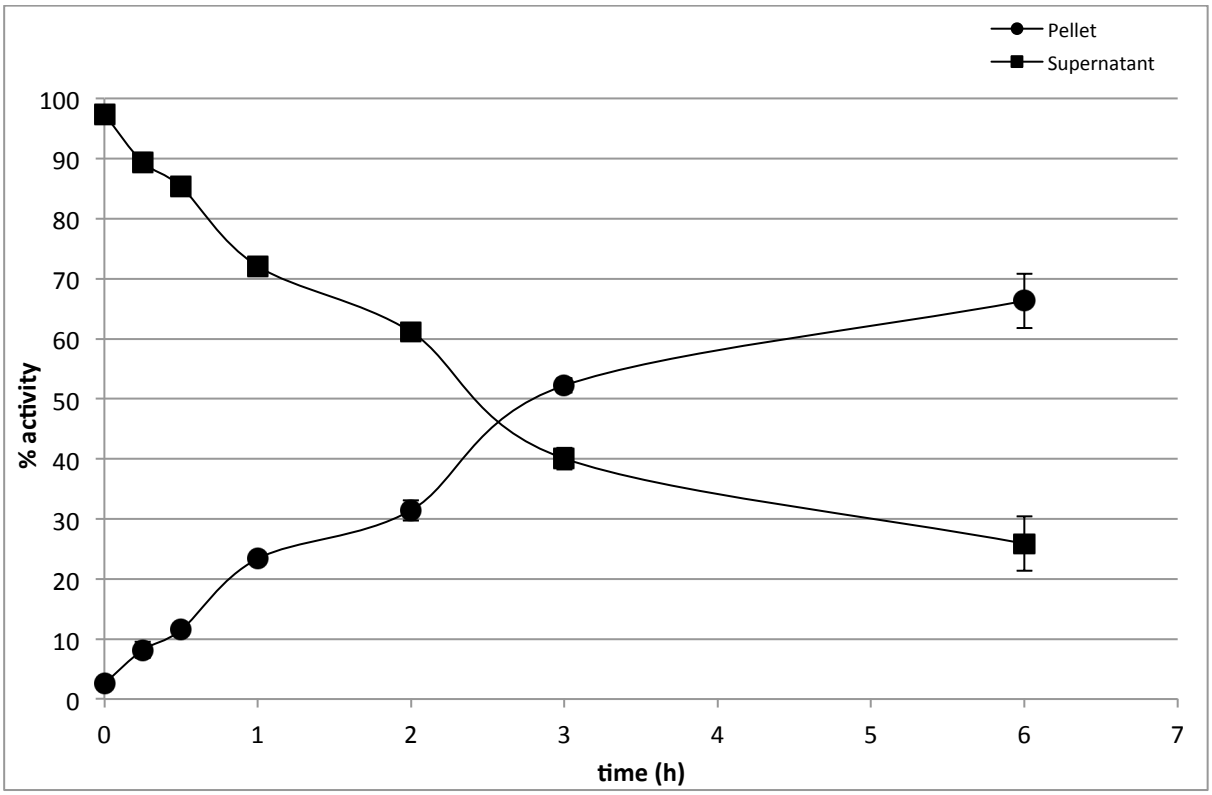

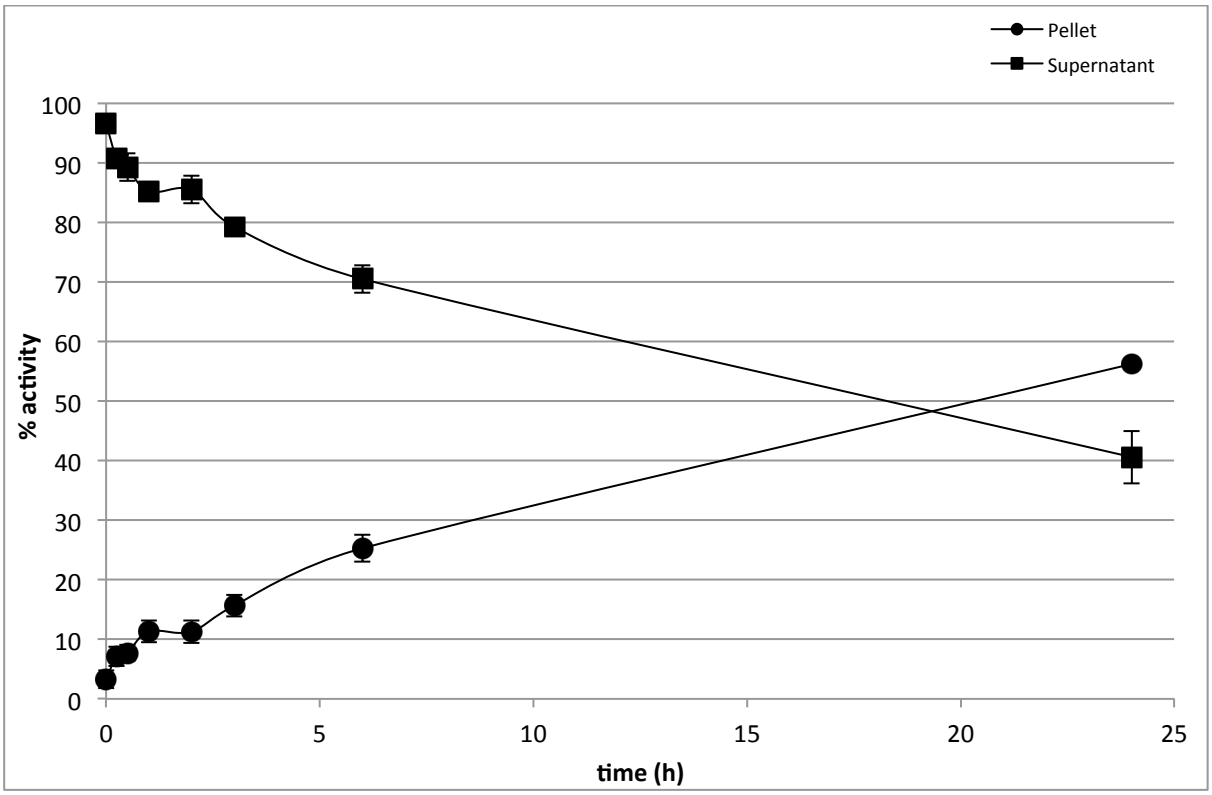

Figure 7: Results of plasma stability studies for 2-4b (top) and 2-5b (bottom). Additional stability data can be found in the supporting information.

The results suggest that the basicity/leaving group ability of the monodentate ligand can be exploited to tune the stability of the $[Tc(CO)_3]^+$ complexes. This can be potentially used to address a long standing concern with tridentate chelate complexes of the tricarbonyl core which are inert to the extent that they do not bind to proteins or other structures within target cells once they are internalized. This can limit the retention of the complex at the site of interest and ultimately the maximum achievable image contrast (i.e. target-to-non-target ratios). In the experiments reported, differences in protein binding

between the complexes due to non-specific binding interactions is unlikely as the complexes all have the same charge and similar log P values (**2-4b** = -0.32, **2-5b** = -0.31, **2-6b** = -0.40, **2-8b** = -1.07).

Cell Uptake Studies

Extensive work has gone into developing Re luminophore and several elegant articles on their use as cellular imaging probes have been reported.[20-28] The Re complex **2-7a** for example was effectively imaged in MCF-7 breast cancer cells (Figure 8) and co-localization experiments performed which match that reported in the literature (see supporting information for images).[4] The advantage of having an isostructural complex derived from ^{99m}Tc is that the radioactive compound can be used to quantitate cell uptake directly without worrying about the impact of the environment on fluorescence intensity.

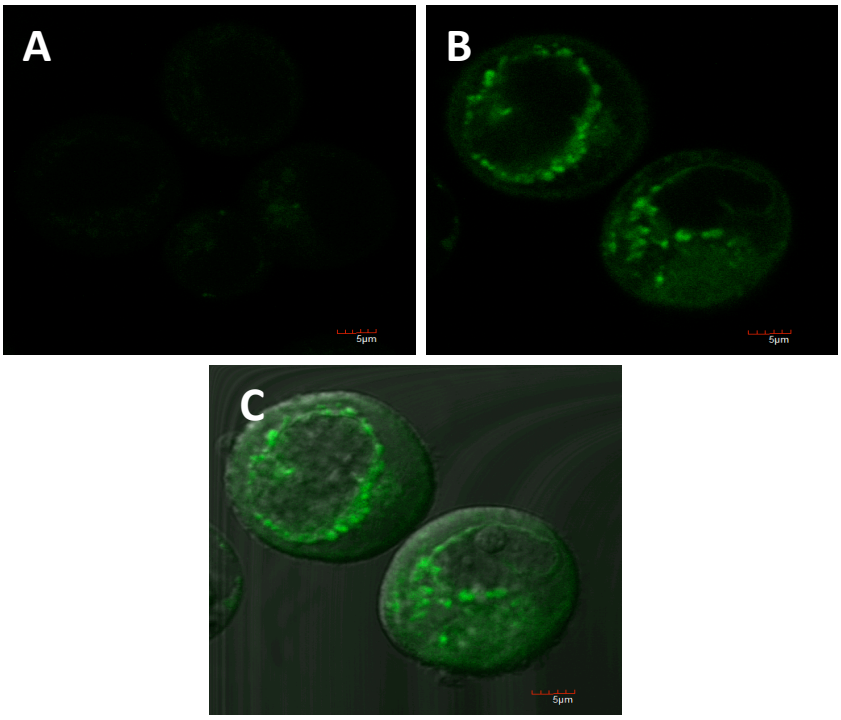

Figure 8: Confocal images of 100 µg/mL 2-7a incubated with $5.0x10^5$ MCF-7 cells for 1.5 h at room temperature. A) Autofluorescence control B) Confocal fluorescence image C) Merged brightfield and fluorescence image.

To demonstrate this, the uptake of the ^{99m}Tc analogue of **2-6a**, which is reported to stain the mitochondria,[4] was measured in the MCF-7 cells. The uptake of **2-6b** was approximately 2% of the incubated activity at 20 min. and 7% at 120 min (Figure 9). When cells were washed with dilute HCl only a small fraction was bound to the cell membrane and the majority of the agent had internalized. For **2-7b** there was approximately 3% uptake at 30 min. and 5% uptake at 120 min (Figure 10). To see if increasing the concentration of the agent would enhance the amount of uptake, cells were incubated with 125 µM of **2-7a** and the ^{99m}Tc complex simultaneously. At 30 min. the

added mass had a statistically significant impact on uptake (nearly double) at the early time point; however there was much less of an effect on the overall uptake at 120 min.

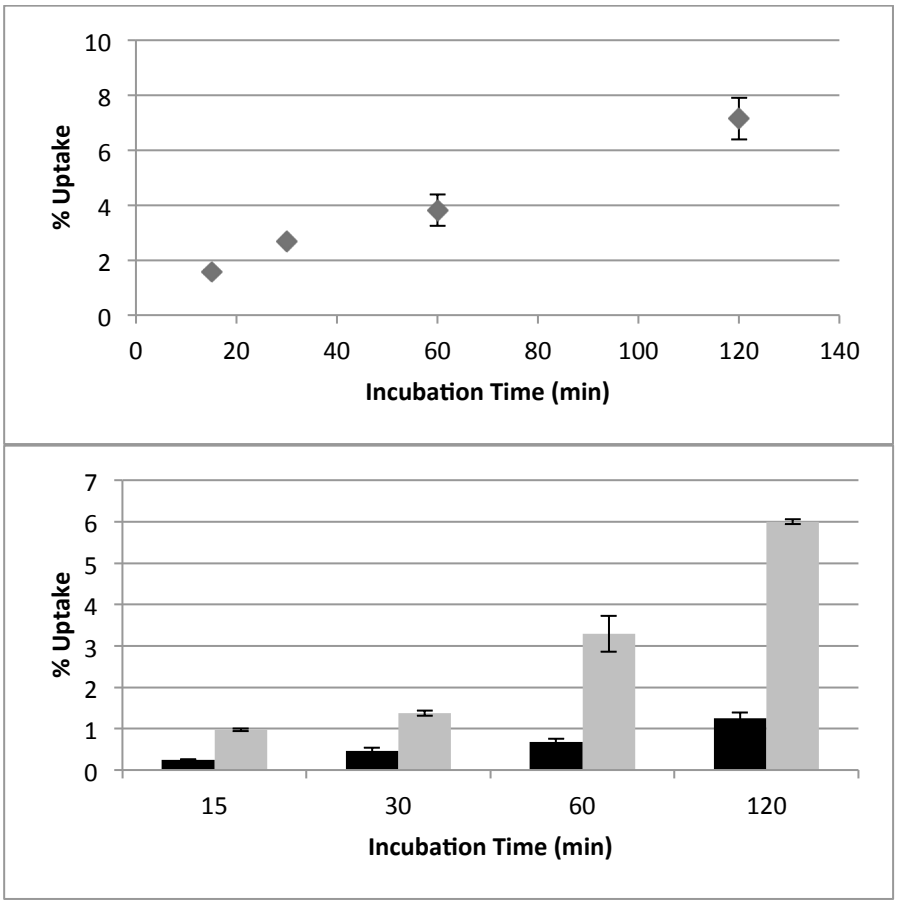

Figure 9: (Top) Percent uptake of 2-6b in MCF-7 cells as a function of incubation time. (Bottom) Results from acid wash experiments indicating the amount of 2-6b externally bound (black bars) and internally bound (grey bars) as a function of time.

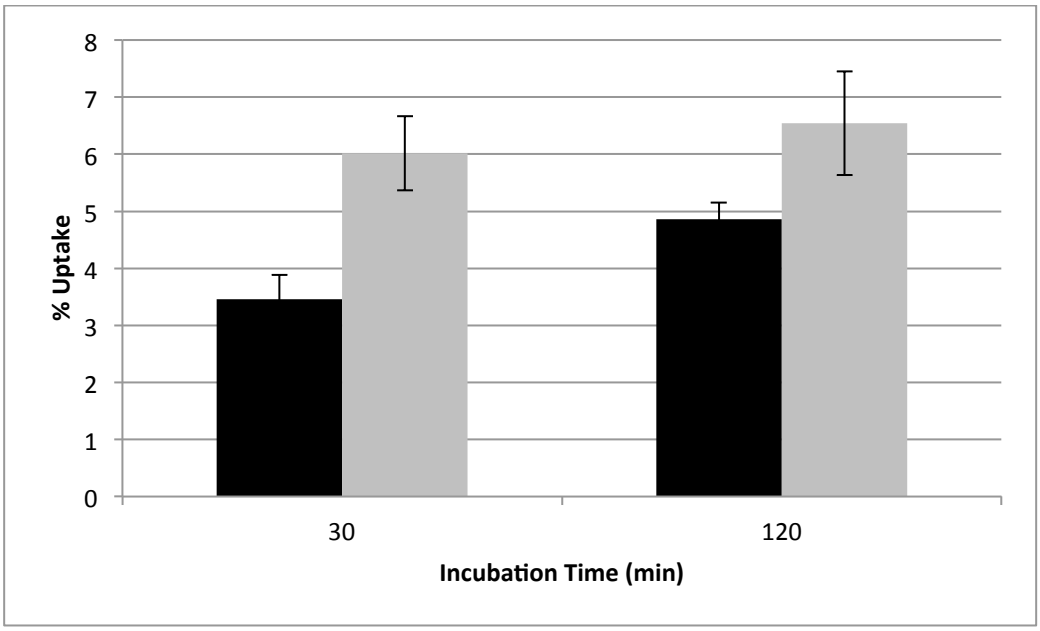

Figure 10: Percent uptake of 2-7b in MCF-7 cells at 30 and 120 min. (black bars). The experiment was repeated in the presence of 2-7a (grey bars).

Targeted Agents

One of the advantages of the [2+1] concept is that pyridine donors can be incorporated into a wide range of targeting vectors without the need to use complex protecting group chemistry. As an initial example, risedronic acid, a pyridine containing bisphosphonate derivative that is used to treat osteoporosis, was used as a vector to create a luminescent analogue of Tc-MDP (**Scheme 2**).

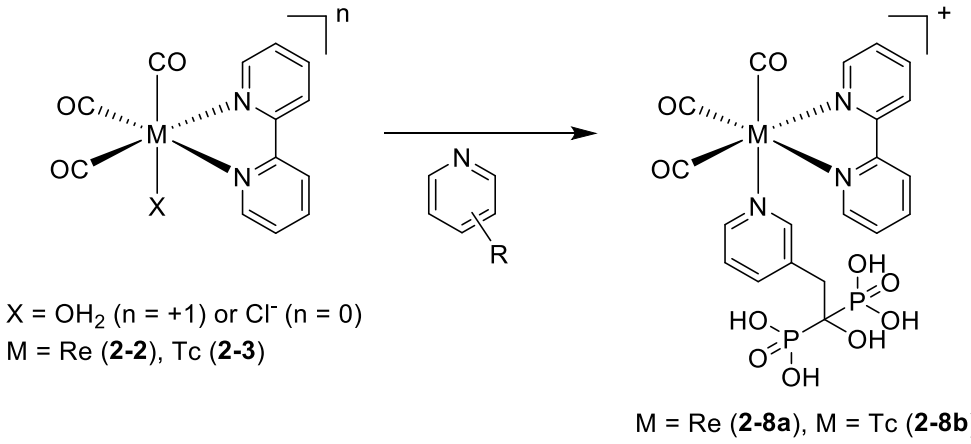

Scheme 2. Synthesis of isostructural Re(I) and ^{99m}Tc complexes with risedronic acid.

For the Re complex, $[Re(CO)_3(bipy)(H_2O)][CF_3SO_3]$ was combined with risedronic acid at pH 7 and the mixture heated at 75 °C overnight. The product was isolated in high yield (70%) by semi-preparative HPLC. MS of the product was consistent with the proposed mass where N coordination was confirmed by ^{1}H NMR spectroscopy. Coordination to Re(I) through the phosphonate groups is possible as has been shown for other transition metal complexes,[38-40] however ^{1}H NMR showed that the aromatic protons in close proximity to the pyridine nitrogen exhibit significant chemical shift changes upon complexation with Re(I) when compared to that of the free ligand. ^{31}P NMR showed the chemical shift of phosphorus to be the same as that in the free ligand. This suggests that the phosphonates are not coordinated to the metal. Unfortunately, attempts to grow single crystals of **8a** were unsuccessful. Nevertheless, compound **2-8a** when excited at 364 nm showed a peak emission at 574 nm which is similar to that for compounds **2-6a** and **2-7a**.

For the Tc complex **2-8b**, [^{99m}Tc(CO)$_3$(bipy)Cl] was combined with risedronic acid in water at pH 7 at 45 °C for 30 min. The product could be isolated by HPLC and was obtained in 85% RCY. *In vitro* binding studies to different calcium salts compared to Tc-MDP, the gold standard radiopharmaceutical for imaging bone metastases, was evaluated. As MDP is prepared using an instant kit in the presence of excess ligand, to allow for direct comparison of the *in vitro* screening studies **2-8b** was prepared similarly. Compound **2-8b** showed comparable binding to hydroxyapatite and dibasic calcium phosphate and superior binding to calcium carbonate. Interestingly MDP more effectively bound calcium pyrophosphate and calcium oxalate (Figure 11). Differences of this nature for MDP and other novel bone seeking radiopharmaceuticals have been reported previously.[41] The utility of **2-8a** and **2-8b** for doing correlated *in vitro* and *in vivo* imaging of bone metastases in the appropriate cell and animal models will be reported separately in due course.

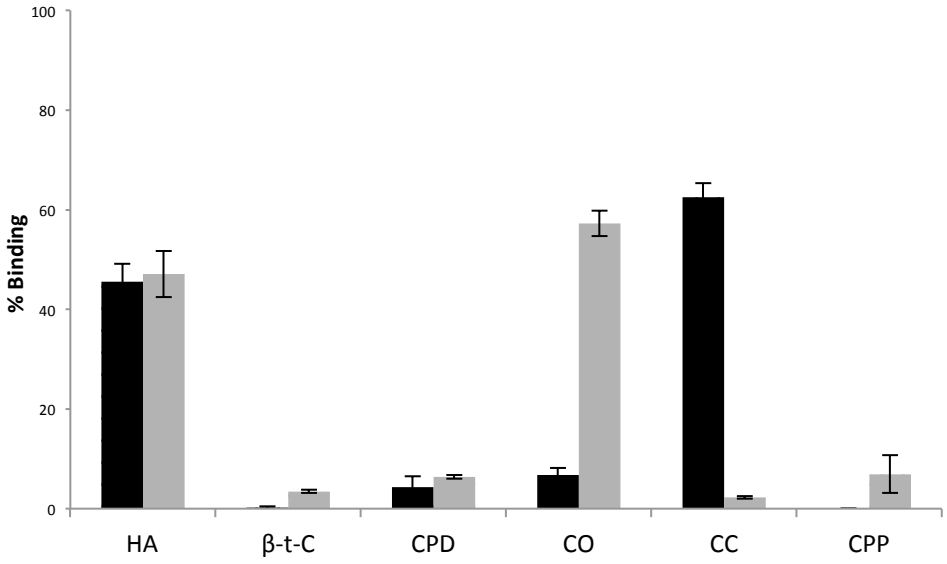

Figure 11: *In vitro* calcium salt binding comparison between [^{99m}Tc(CO)$_3$(bipy)(RA)] (2-8b) (black bars) and ^{99m}Tc-MDP (grey bars). HA = hydroxyapatite, β-t-C = β-tri-calcium phosphate, CPD = calcium phosphate dibasic, CO = calcium oxalate, CC = calcium carbonate, CPP = calcium pyrophosphate.

Conclusions

A convenient method to prepare ^{99m}Tc analogues of a class of established rhenium luminophore was developed. The plasma stability of the complexes are impacted by the leaving group ability of the monodentate ligand making it possible to tune the robustness of the complexes and to prepare products using a pH controlled one-pot reaction. The ability to generate the ^{99m}Tc complexes makes it possible to quantitate uptake of the corresponding Re luminophore and evaluate their distribution *in vivo*. As a corollary, the ability to access the fluorescent form of complexes will be a useful tool in validating the molecular mechanisms of targeted Tc probes derived from the [2+1] construct. There are an increasing number of Re luminophore being developed which have different

bifunctional ligands beyond bipy and enhanced chemical and optical properties.[6,35] Furthermore, Alberto and coworkers have already demonstrated the potential utility of a [2+1] strategy by combining a targeting vector with a nuclear targeting interchelator linked via a M(I) core.[42] With the methods reported here it will be possible to use one-pot or two-step labelling reactions to create new families of targeted [2+1] type isostructural fluorescent and nuclear probes.

Experimental Section

General. Unless otherwise noted, all reagents and solvents were ACS grade and used without further purification from commercial suppliers. 2,2′-Bipyridine, pyridine, 4-dimethylaminopyridine, 3-pyridinemethanol (PM), nicotinic acid, cyclohexanol, silver trifluoromethanosulfonate, and $Re(CO)_5Br$ were purchased from Sigma Aldrich. Tetrahydrofuran, acetone and methanol were purchased from Caledon. Risedronic (RA) acid was purchased from Santa Cruz Biotechnology, Inc. Distilled water was used for all experiments. Compounds **2-4a**, **2-5a**, **2-6a** and **2-7a** were prepared according to literature methods.[32,33] Triflate salts were converted to the corresponding chlorides using Bio-Rad Prefilled Poly Prep columns containing AG 1-X8 (100-200) chloride ion exchange resin. ^{99m}Tc was obtained as TcO_4^- from a $^{99}Mo/^{99m}Tc$ generator (Lantheus Medical Imaging) in saline (0.9 % NaCl). *Caution*: *^{99m}Tc is a γ-emitter ($E\gamma$ = 140 keV, $t_{1/2}$ = 6 h) and should only be used in a licensed and appropriately shielded facility*.

^1H, ^{13}C and ^{31}P spectra were recorded on a Bruker Avance AV-600 instrument at 300 K. High Resolution Mass Spectra (HRMS) were collected on a Waters/Micromass Q-

Tof Global Ultima spectrometer. Microwave reactions were performed on a Biotage Initiator 60 instrument. High Performance Liquid Chromatography (HPLC) was performed using a Waters XBridge analytical column (5 µm, 4.6 x 100 mm, phenyl) or XBridge prep column (5 µm, 10 x 100 mm, C18) with a Waters 1525 system connected to a Bioscan γ detector and a 2998 photodiode array detector monitoring at 254 nm operated using the Empower software package. Flow rates were 1 mL/min. (analytical) or 4 mL/min. (prep) using the following methods: Method A: Solvent A: water + 0.1% TFA; Solvent B: acetonitrile + 0.1% TFA. Gradient: 10% B (0-2 min.), 100% B (2-12 min.), 100% B (12-14 min.), 10 % B (14-16 min.), 10%B (16-20 min). Method B: Solvent A: water + 0.1% TFA; Solvent B: acetonitrile + 0.1% TFA. Gradient: 10% B (0-2 min.), 100% B (2-12 min.), 100% B (12-14 min.), 10 % B (14-15 min.). Method C: Solvent A: 0.4% ammonium formate (w/v) in water; Solvent B: acetonitrile. Gradient: 10% B (0-2 min.), 100% B (2-12 min.), 100% B (12-14 min.), 10% B (14-15 min.).

Cell Culture and Processing: MCF-7 breast adenocarcinoma cells *(*ATCC no. HTB-22) were cultured in Dulbecco's modified eagle medium (DMEM) supplemented with 10% fetal bovine serum and 1% penicillin streptomycin. The cell line was maintained at 37 °C and 5% CO_2. The buffer used for the MCF-7 cell uptake assay consisted of DMEM growth media and 0.5% bovine serum albumin (BSA). RIPA buffer was prepared with 100 mM Tris pH 8, 50 mM NaCl, 1% NP40, 0.5% sodium deoxycholate and 0.1% SDS (Bioshop). Two solutions were required for the hydrochloric acid wash on the MCF-7 cells. *Solution 1* was comprised of 50 mM Glycine HCl and 100 nM NaCl. *Solution 2* was made up of 0.5 M HEPES and 100 nM NaCl. Confocal images were generated using an

Olympus FluoView 1000 Laser Scanning Confocal Microscope at the wavelengths indicated.

[Re(CO)$_3$(bipy)(CHN)][CF$_3$SO$_3$] ***(2-7a)***. Compound **2-7a** was prepared according to the literature method with minor modifications.[33] Cyclohexyl nicotinate (30 mg, 0.15 mmol) was dissolved in DCM (5 mL) and added to [Re(CO)$_3$(bipy)(CH$_3$CN)][CF$_3$SO$_3$] (62 mg, 0.10 mmol) in DCM (10 mL) and heated at 60 °C overnight. The formation of the desired product was confirmed by TLC (DCM/MeOH=10:1). The crude reaction mixture was then purified by column chromatography using DCM/MeOH = 10:1 as eluent to obtain the product as a yellow solid. Characterization data matched that found in the literature. Yield: 40 mg (52%).

[Re(CO)$_3$(bipy)(RA)][CF$_3$SO$_3$] ***(2-8a)***. The pH of a solution of freshly prepared [Re(CO)$_3$(bipy)(H$_2$O)][CF$_3$SO$_3$] (50 mg, 0.08 mmol) in water (10 mL) was adjusted to 7 with 0.1 M NaOH and added with constant stirring to a solution of risedronic acid (25.0 mg, 0.09 mmol) in water (5 mL) which had been adjusted to pH 7 with 0.1 M NaOH. The reaction mixture was then heated at 75 °C overnight whereupon the solution was allowed to cool to room temperature and concentrated to dryness by rotary evaporation leaving a yellow solid. Unreacted starting material was removed by the addition of CH_2Cl_2 (5 mL) followed by filtration. The residue was dissolved in MeOH and the product isolated (40 mg, 70%) as a yellow solid by semi-preparative HPLC (Method C). m.p. 200^{o}C (decomp.). ^{1}H NMR (D$_2$O, 600 MHz): δ (ppm) 9.25 (d, 2H, Ar-H); 8.38 (s, 1H, Ar-H);

8.32 (d, 2H, Ar-H); 8.23 (s, 1H, Ar-H); 8.17 (t, 2H, Ar-H); 8.07 (d, 1H, Ar-H); 7.79 (d, 1H, Ar-H); 7.71 (q, 2H, Ar-H); 7.07 (q, 1H, Ar-H); 3.01 (t, 2H, -CH2-). ^{31}P NMR (D_2O, 242 MHz): δ (ppm) 16.83. ^{19}F (D_2O, 470 MHz): δ (ppm) -75.5 (s, CF_3SO_3). HRMS (ESI+) m/z calcd for $C_{20}H_{19}N_3O_{10}P_2Re$ [M-CF_3SO_3]: 710.01 $[M + H]^+$, found: 710.01. HRMS (ESI-) m/z calcd for $C_{20}H_{19}N_3O_{10}P_2Re$ [M-CF3SO3]: 708.01 [M - H], found: 707.99. HPLC (UV 254 nm, Method C) R_t = 6.5 min.

General Procedure for the Preparation of $[^{99m}Tc(CO)_3(bipy)(L)]^+$. Sodium boranocarbonate (10.0 mg, 0.10 mmol), sodium carbonate (15.0 mg, 0.14 mmol), sodium borate (20 mg, 0.05 mmol) and sodium potassium tartrate (22 mg, 0.08 mmol) were placed in a microwave vial and purged with argon for 10 min. To this mixture, Na[$^{99m}TcO_4$] (1 mL) was added and the vial was heated in a microwave at 110 °C for 3.5 min. to form $[^{99m}Tc(CO)_3(H_2O)_3]^+$. The solution was cooled, the pH adjusted to 6 with 0.1 M HCl (0.2 mL) and the solution added to bipyridine (1 mg, 6 mmol) in a 5 mL microwave vial, which had been purged with argon. The reaction mixture was stirred at 40 °C for 30 min. and the solution added to one of the monodentate ligands (300 – 500 mmol) under argon and the mixture stirred at 40 °C for 20 min. to give $[^{99m}Tc(CO)_3(bipy)(L)]^+$. The formation of products was confirmed by analytical HPLC using the HPLC methods A (**2-4b** and **2-5b**) or C (**2-6b** and **2-7b**). **2-4b**: R_t = 8.6 min, RCY = 90±2% (n = 3); **2-5b**: R_t = 9.7 min, RCY = 87±3% (n = 3); **2-6b**: R_t = 8.3 min, RCY = 83±2% (n = 3); **2-7b**: R_t = 11.1 min, RCY = 17±5% (n = 3).

Purification of ^{99m}Tc Complexes. Purification of [^{99m}Tc(CO)$_3$(bipy)Cl] and the [^{99m}Tc(CO)$_3$(bipy)(L)]$^+$ (**2-4b** - **2-6b**) was achieved by solid phase extraction (SPE) or semi-preparative HPLC. For SPE, the reaction mixture was diluted with water (2 mL) and then loaded on a Waters C18 Sep-Pak Plus cartridge, which had been activated with EtOH (1 x 6 mL) followed by H_2O (1 x 6 mL). After loading the reaction mixture, the column was washed with 15 % ACN in H_2O (2 x 6 mL), followed by 25 % ACN in 0.4 % (w/v) aqueous ammonium formate (1 x 6 mL). The desired products were eluted with a 1:1 v/v mixture of 0.4 % aqueous ammonium formate and ACN.

One-pot Synthesis of [^{99m}Tc(CO)$_3$(bipy)(DMAP)]$^+$ ***(2-5b)***. [^{99m}Tc(CO)$_3$(H$_2$O)$_3$] was added to an argon purged solution of bipyridine (1 mg, 6 mmol) and DMAP (40 mg, 330 mmol) in water (0.5 mL). The pH of the solution was adjusted to 2 with 0.1 M HCl and the mixture stirred at 40 °C for 15 min. whereupon the pH of the solution was adjusted to 9 with 1 M NaOH and the reaction mixture stirred at 40 °C for 30 min. A single product (R_t = 10.1 min.) was observed in the gamma trace and the product was isolated in 80% yield by HPLC (Method B).

[^{99m}Tc(CO)$_3$(bipy)(RA)] ***(2-8b)***. The pH of a solution of [^{99m}Tc(CO)$_3$(bipy)Cl] (370 MBq) was adjusted to 7 with 1 M NaOH and added to an argon purged solution of risedronic acid in water (88 μM) whose pH was adjusted to 7 with 1M NaOH. The reaction mixture was stirred at 45 °C for 30 min. and the product isolated by semi-preparative HPLC (Method C): R_t = 6.5 min, RCY = 85±3% (n = 3).

Plasma Stability. 100 µL (111 MBq) of the ^{99m}Tc complex was added to 900 µL of pre-warmed (37˚C) mouse plasma (Innovative Research, IMS-CD1-N), and the mixture vortexed and incubated at 37˚C. At each time point (t=0, 0.25 h, 0.5 h, 1 h, 2 h, 3 h, 6 h for **2-4b** and t=0, 0.25 h, 0.5 h, 1 h, 2 h, 3 h, 6 h, 24 h for **2-5b**), a sample (100 µL) was removed and added to ice cold acetonitrile (200 µL). The resulting mixture was vortexed and then centrifuged at maximum speed (15,000 rpm) for 10 min. The amount of activity in the sample was measured using a dose calibrator (Capintec Inc, CRC-25R). The supernatant was separated from the pellet and the activity from the supernatant and the pellet measured separately. For all time points except t=0, pellets were washed with ice cold PBS (50 µL) prior to measuring the activity. The experiment was performed in duplicate and the percent bound to blood proteins calculated as follows: [(amount of activity in washed pellet)/(amount of activity in unwashed pellet)+(amount of activity in supernatant)] × 100%. The values reported are an average of the two experiments ± standard deviation.

MCF-7 Uptake Assay. MCF-7 cells were detached from the flask using trypsin-EDTA and were re-suspended in buffer consisting of DMEM growth media and 0.5% BSA. Six 1 mL aliquots containing 5.0×10^5 cells in suspension and 33.3 kBq of either **2-6b** or **2-7b** were prepared for each incubation time point. These aliquots were incubated at 37 ˚C for the specified time. Following the incubation period, the supernatant was removed, and the cells were washed three times with PBS. On the remaining three aliquots, a hydrochloric

acid wash was performed. The cells were re-suspended in the HCl wash solution 1 and gently vortexed for three min. The cells were then treated with HCl wash solution 2. The supernatant was removed, and cells were washed an additional three times with PBS before being re-suspended in RIPA buffer and incubated at 37˚C for 30 min. All cells and supernatants were transferred to gamma tubes and counted for one min. using an automated gamma counter. This experiment was repeated whereby 125 μM of **2-7a** was incubated along with **2-7b**.

Confocal Microscopy. MCF-7 cells were removed from the flask using trypsin-EDTA. The cells were distributed into aliquots containing $5.0x10^5$ cells and 100 μg of the either **2-6a** or **2-7a** (or equivalent volume of DMSO for the control) in 1 mL DMEM media. The aliquots were incubated at room temperature for 1.5 h after which they were washed three times with PBS. The cells were re-suspended in 100 μL PBS and mounted on the slide for imaging. Cell images were obtained by excitation at 405 nm and emission collection from 562 – 601 nm; PlanApo 60x oil, NA 1.4 lens and a zoom factor of 4 was applied.

Hydroxyapatite Binding. The method for *in vitro* calcium salt binding followed a literature procedure.[39] Briefly, 10 μL (0.8 MBq) of either **2-8b** or ^{99m}Tc-MDP (as a positive control) was added to 1.5 mL of 1 mg/mL solutions of hydroxyapatite, β-tri-calcium phosphate, calcium phosphate dibasic, calcium oxalate, calcium carbonate and calcium pyrophosphate in a 50 mM Tris buffer (pH 6.9). A no salt control was also

included. Samples were incubated with gentle shaking for 1h at room temperature and then centrifuged for 5 min. at 10 000 rpm. A 60 µL aliquot of the supernatant was counted using a gamma counter. The percent binding was calculated using the following formula, where CPMs are the counts per min. of each sample and the CPMc are the counts per min. for the no salt control:

$$\%\ binding = \left(1 - \frac{CPMs}{CPMc}\right) x100$$

The reported percent binding values are an average of two experiments done in triplicate.

2.6 Colocalization Studies

Having established the utility of the [2+1] constructs, the focus shifted towards evaluation of the Re complex versus other known mitochondrial targeted fluorophores. Following the incubation conditions outlined by Fernández-Moreira *et al.*, who evaluated uptake of mitochondrial targeted dyes, MCF-7 cells were first incubated with 100 µg/mL of **2-6a** or **2-7a** for 30 min. at 4 ˚C.[4] Confocal microscopy showed uptake in MCF-7 cells for **2-7a**, but not **2-6a**. In order to better visualize the fluorescence uptake of **2-7a**, 100 µg/mL of the compound was incubated with 5.0 x 10^5cells for 1.5 hours at room temperature. **2-6a** was also incubated with MCF-7 cells under these conditions, but once again no fluorescence above autofluorescence levels was observed (Figure 12).

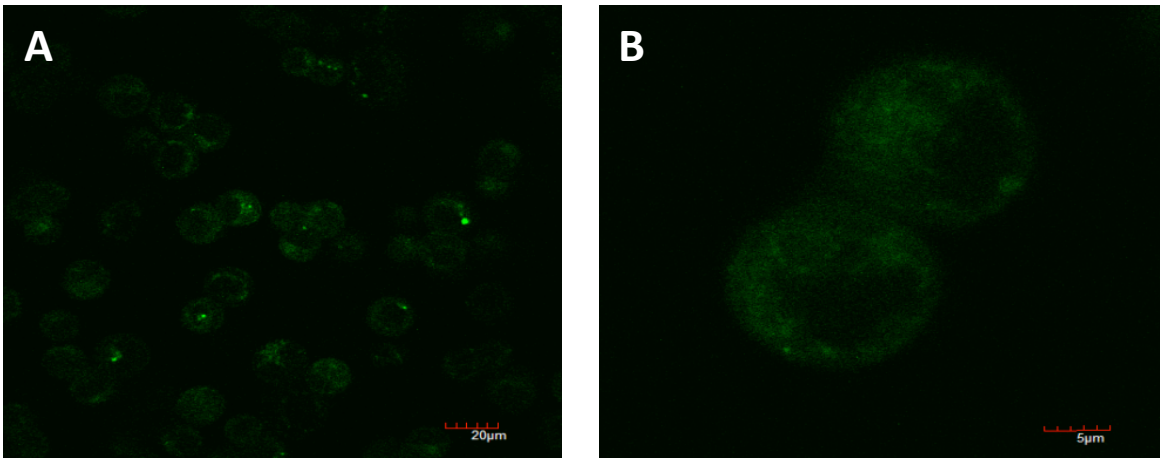

Figure 12: Confocal microscopy images (excitation at 405 nm) A) MCF-7 autofluorescence levels B) MCF-7 cells incubated with 100 µg/mL of **2-6a** for 1.5 h at room temperature.

A colocalization experiment was performed subsequently in order to determine whether **2-7a** localizes in the mitochondria as predicted. Tetramethylrhodamine (TMRE) was initially co-incubated with the rhenium derivatives, however, it was found that the 405 nm laser was also exciting the TMRE and producing fluorescence emission. As a result an alternative mitochondrial dye, MitoTracker Deep Red, was tested for colocalization with **2-7a** (Figure 13). The excitation and emission wavelengths of this dye are better suited for colocalization experiments with the rhenium bipyridine derivatives.

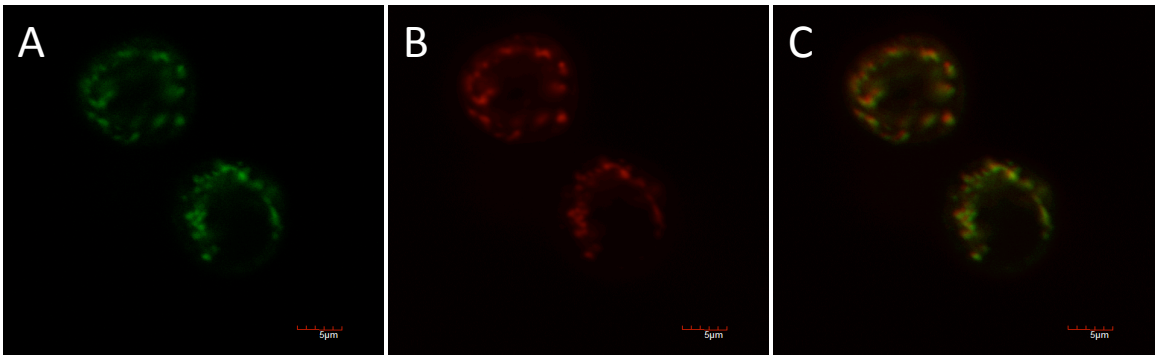

Figure 13: Colocalization of **2-7a** and MitoTracker Deep Red. A) **2-7a** B) MitoTracker Deep Red C) Overlay image

Although overlap was evident in the images of **2-7a** and MitoTracker Deep Red (Figure 13 A and B), quantitative analysis using Pearson's coefficient indicated that there was poor colocalization. Overlaying two images and observing the merging of the two colour channels (Figure 13C), while consistent with correlated uptake, is not always a precise way to ensure that colocalization has occurred. This is associated with the fact that the 2D overlay image is produced from a slice in the z-axis, however this neglects the details of the 3D structure of the cell and the fluorescent probes. Pearson's coefficient is often used as a means of determining the linear correlation between pixel intensity values. A value between -1 and 1 is assigned, with a value of 1 representing positive correlation, a value of -1 representing negative correlation and a value of 0 representing no correlation.[43]

In a case of true colocalization, the signal intensities for each fluorophore are proportionate for all pixels. A scatter plot whereby for each fluorophore the signal intensity of all pixels is created (i.e. channel 1 signal intensities versus channel 2 signal intensities) a linear correlation should be observed, giving a Pearson's coefficient of 1.

One possible explanation for the discrepancy between the imaging data and calculated correlation is that Pearson's coefficient is reduced if the intensity of one channel is low compared to that of the other. The scatter plot in this case would have a shift in the slope of the line generated from the linear correlation of the pixel intensities, increasing closer to the axis represented by the more intense channel. Because of the lower pixel intensities of the one channel, the sensitivity is lowered, creating a greater subpopulation of pixels for the more intense channel. This would result in a poorer linear correlation, and thus a lower value of Pearson's coefficient. Lastly, if the two fluorophore channels partially overlap as in the case of incomplete colocalization, there would be a greater deviation from the average, and thus a weaker linear correlation would be observed.[43] Figure 14 shows a scatter plot for the experimentally obtained colocalization data. A relatively large spread is shown, indicating a decreased Pearson's coefficient.

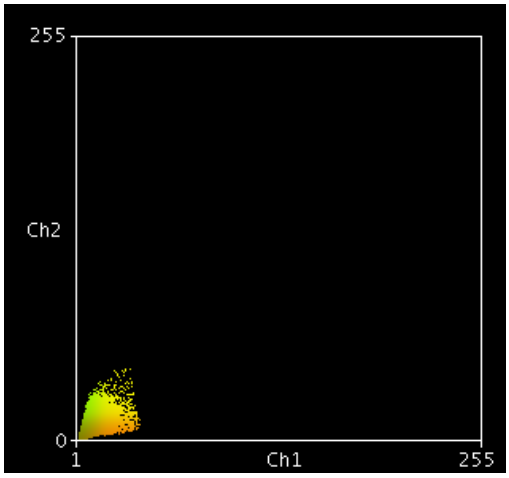

Figure 14: Scatter plot showing signal intensities of the rhenium bipyridine compound (Ch2) versus the signal intensities of the MitoTracker Deep Red (Ch1).

Another possible reason for the poor colocalization observed in Figure 13 could be the result of sample motion between acquisitions with the two different lasers. The original experiment was performed with the cells in suspension and not adhered to the plate, so when mounted on the slide they could potentially shift. In order to try and minimize movement of the cells once on the slide, fixing with paraformaldehyde (PFA) and mounting with agar solution were attempted. These methods however did not improve the value of Pearson's coefficient.

An additional consideration is that Fernández-Moreira *et al.* speculated that although **2-7a** most likely does get taken up into the mitochondria due to the mitochondrial membrane's potential gradient, the compound likely also gets taken up into other lipophilic cellular structures. If this were true, the cell image would have pixels in which **2-7a** is present but in which MitoTracker Deep Red is not. This would represent a case of incomplete colocalization, and Pearson's coefficient would be low. Therefore, although **2-7a** would have localized in the mitochondria, the presence of the compound elsewhere in the cell even in trace amounts would result in a relatively low value of Pearson's coefficeint.

2.7 Turn On Probes

One way to achieve high contrast for the optical probes is to have them be optically silent until they bind their target of interest or have been metabolized in the cells of interest. For

example, Zhang *et al*. have developed a set of Ru(II)-bipyridine complex derivatives attached to a 2,4-dinitrophenyl (DNP) group. The fluorescence of the Ru(II)-bipyridine complex is quenched when attached to DNP due to a photoinduced electron transfer (PET) process. When reacted with thiophenol, the DNP is cleaved, and fluorescence is restored.[44]

More recently, the [2+1] ligands developed in the Valliant lab were adapted in order to create an activatable optical probe that would act as a switch and turn on a fluorescent signal when cleaved by a specific biological agent associated with the diseased cells of interest. DNP was linked to a [2+1] derivative as shown in Figure 15 (compound **2-9**), in order to quench the fluorescence. When DNP is cleaved, the fluorescence should be restored.

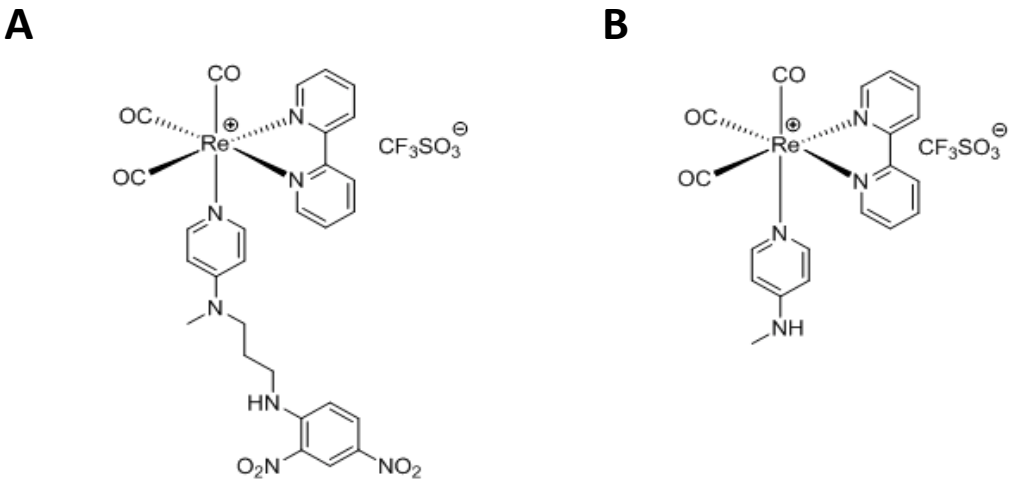

Figure 15: A) Compound **2-9**: Fluorescence is quenched by the addition of DNP B) Following the cleavage of DNP, the construct should be fluorescent (compound **2-5a**).

The peak emission from 500 μM of both **2-9** and **2-5a** were measured with the Tecan Infinite M1000 plate reader (Figure 16). As shown, the peak fluorescence intensity is approximately 50% lower for the compound including the DNP. This shows that DNP is effectively quenching the fluorescence of the [2+1] ligand.

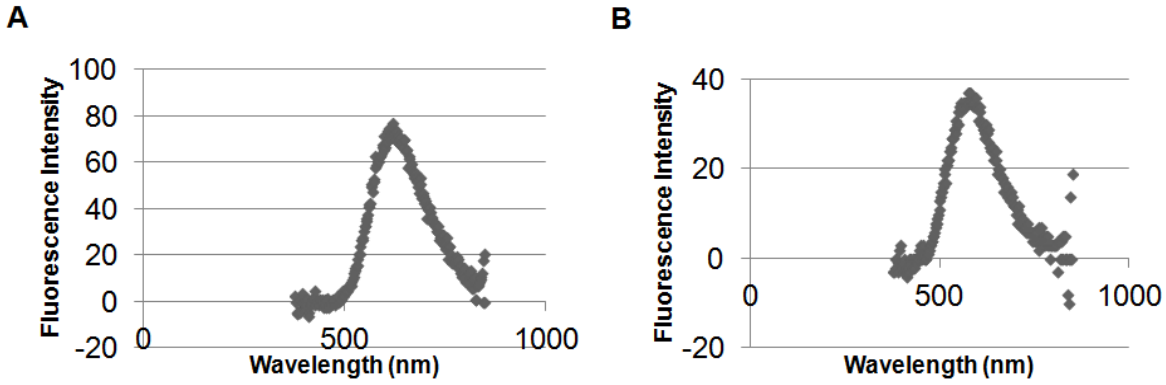

Figure 16: A) Fluorescence intensity for **2-5a** when excited at 365 nm. B) Fluorescence intensity of **2-9** when excited at 365 nm.

In order to displace the DNP and restore fluorescence to the construct, 10-fold excess DMAP was added and fluorescence intensity was measured up to three hours after. No increase in fluorescence was observed, and mass spectrometry also showed that **2-9** was still intact. Work is ongoing on optimizing the linker chemistry. In addition, the use of a different quencher will be valuable, as the absorption spectrum of the DNP and the fluorescence emission spectrum for **2-9** overlap to a limited extent.[45] Tetrazine may be more appropriate for fluorophores emitting in the range of 510-570 nm and should therefore increase the quenching and fluorescence intensity ratio.[46] For example, Devaraj *et al.* showed that attaching the fluorescent dye BODIPY TMR-X (peak fluorescence

emission of 573 nm) to tetrazine quenched the fluorescence. The fluorescence was shown to increase 20.6-fold with the cycloaddition of trans-cyclooctene (TCO).[47]

2.8 Conclusion

The [2+1] ligands were prepared as an alternative to the SAACIII ligand in order to have a probe with a longer peak fluorescence emission wavelength. The Valliant group adapted the previously reported luminescent rhenium analogues to incorporate ^{99m}Tc, thereby creating a nuclear analogue.[4] The rhenium analogues were assessed for use as an optical probe through confocal microscopy, and the ^{99m}Tc analogues were evaluated for percent uptake in MCF-7 cells. The results showed that the complexes are useful dual purpose probes and can be used to create a new generation of isostructural optical and nuclear imaging agents.

2.9 References

1 Pitchumony, T. S., Banevicius, L., Janzen, N., Zubieta, J. & Valliant, J. F. Isostructural nuclear and luminescent probes derived from stabilized [2 + 1] rhenium(i)/technetium(i) organometallic complexes. *Inorg Chem* **52**, 13521-13528 (2013).

2 Stephenson, K. A. *et al.* A new strategy for the preparation of peptide-targeted radiopharmaceuticals based on an fmoc-lysine-derived single amino acid chelate (SAAC). automated solid-phase synthesis, NMR characterization, and in vitro

screening of fMLF(SAAC)G and fMLF[(SAAC-Re(CO)3)+]G. *Bioconjug Chem* **15**, 128-136 (2004).

3 Stephenson, K. A. *et al.* Bridging the gap between in vitro and in vivo imaging: isostructural Re and 99mTc complexes for correlating fluorescence and radioimaging studies. *J Am Chem Soc* **126**, 8598-8599 (2004).

4 Fernandez-Moreira, V. *et al.* Uptake and localisation of rhenium fac-tricarbonyl polypyridyls in fluorescent cell imaging experiments. *Org Biomol Chem* **8**, 3888-3901 (2010).

5 Amoroso, A. J. *et al.* 3-Chloromethylpyridyl bipyridine fac-tricarbonyl rhenium: a thiol-reactive luminophore for fluorescence microscopy accumulates in mitochondria. *New J Chem* **32**, 1097-1102 (2008).

6 Spagnul, C. *et al.* Novel water-soluble 99mTc(I)/Re(I)-porphyrin conjugates as potential multimodal agents for molecular imaging. *J Inorg Biochem* **122**, 57-65 (2013).

7 Thorp-Greenwood, F. L. & Coogan, M. P. Multimodal radio-(PET/SPECT) and fluorescence imaging agents based on metallo-radioisotopes: current applications and prospects for development of new agents. *Dalton Trans* **40**, 6129-6143 (2011).

8 Jennings, L. E. & Long, N. J. 'Two is better than one'-probes for dual-modality molecular imaging. *Chem Commun*, 3511-3524 (2009).

9 Kobayashi, H., Longmire, M. R., Ogawa, M. & Choyke, P. L. Rational chemical design of the next generation of molecular imaging probes based on physics and biology: mixing modalities, colors and signals. *Chem Soc Rev.* **40**, 4626-4648 (2011).

10 Morais, G. R., Paulo, A. & Santos, I. Organometallic Complexes for SPECT Imaging and/or Radionuclide Therapy. *Organometallics* **31**, 5693-5714 (2012).

11 Ghosh, S. C. *et al.* Multimodal Chelation Platform for Near-Infrared Fluorescence/Nuclear Imaging. *J Med Chem* **56**, 406-416 (2012).

12 Priem, T. *et al.* A novel sulfonated prosthetic group for F-18 -radiolabelling and imparting water solubility of biomolecules and cyanine fluorophores. *Org Biomol Chem* **11**, 469-479 (2013).

13 Li, Z. *et al.* Rapid aqueous [18F]-labeling of a bodipy dye for positron emission tomography/fluorescence dual modality imaging. *Chem Commun* **47**, 9324-9326 (2011).

14 Botchway, S., Dilworth, J. R. & Salichou, M. One and two photon fluorescent complexes of rhenium and their technetium analogues. *Dalton Trans* **39**, 5219-5220 (2010).

15 Boulay, A. *et al.* First dinuclear Re/Tc complex as a potential bimodal Optical/SPECT molecular imaging agent. *Dalton Trans* **40**, 6206-6209 (2011).

16 Clede, S. *et al.* A rhenium tris-carbonyl derivative as a single core multimodal probe for imaging (SCoMPI) combining infrared and luminescent properties. *Chem Commun* **48**, 7729-7731 (2012).

17 Schaffer, P. *et al.* Isostructural fluorescent and radioactive probes for monitoring neural stem and progenitor cell transplants. *Nucl Med Biol* **35**, 159-169 (2008).

18 Banerjee, S. R., Babich, J. W. & Zubieta, J. Site directed maleimide bifunctional chelators for the M(CO)3+ core (M = 99mTc, Re). *Chem Commun*, 1784-1786 (2005).

19 Gasser, G. *et al.* Synthesis, characterisation and bioimaging of a fluorescent rhenium-containing PNA bioconjugate. *Dalton Trans* **41**, 2304-2313 (2012).

20 Lo, K. K.-W., Choi, A. W.-T. & Law, W. H.-T. Applications of luminescent inorganic and organometallic transition metal complexes as biomolecular and cellular probes. *Dalton Trans* **41**, 6021-6047 (2012).

21 Lo, K. K.-W., Zhang, K. Y. & Li, S. P.-Y. Recent Exploitation of Luminescent Rhenium(I) Tricarbonyl Polypyridine Complexes as Biomolecular and Cellular Probes. *Eur J Inorg Chem* **2011**, 3551-3568 (2011).

22 Louie, M.-W., Liu, H.-W., Lam, M. H.-C., Lam, Y.-W. & Lo, K. K.-W. Luminescent Rhenium(I) Polypyridine Complexes Appended with an α-D-

Glucose Moiety as Novel Biomolecular and Cellular Probes. *Chemistry* **17**, 8304-8308 (2011).

23 Louie, M.-W., Choi, A. W.-T., Liu, H.-W., Chan, B. T.-N. & Lo, K. K.-W. Synthesis, Emission Characteristics, Cellular Studies, and Bioconjugation Properties of Luminescent Rhenium(I) Polypyridine Complexes with a Fluorous Pendant. *Organometallics* **31**, 5844-5855 (2012).

24 Kam-Wing Lo, K., Chun-Ming Ng, D., Hui, W.-K. & Cheung, K.-K. Luminescent rhenium(i) polypyridine complexes with an isothiocyanate moiety-versatile labelling reagents for biomolecules. *J Chem Soc, Dalton Trans*, 2634-2640 (2001).

25 Choi, A. W.-T. *et al.* Emissive Behavior, Cytotoxic Activity, Cellular Uptake, and PEGylation Properties of New Luminescent Rhenium(I) Polypyridine Poly(ethylene glycol) Complexes. *Inorg Chem* **51**, 13289-13302 (2012).

26 Fernández-Moreira, V. *et al.* Bioconjugated Rhenium(I) Complexes with Amino Acid Derivatives: Synthesis, Photophysical Properties, and Cell Imaging Studies. *Organometallics* **31**, 5950-5957 (2012).

27 Thorp-Greenwood, F. L. An Introduction to Organometallic Complexes in Fluorescence Cell Imaging: Current Applications and Future Prospects. *Organometallics* **31**, 5686-5692 (2012).

28 Choi, A. W.-T., Poon, C.-S., Liu, H.-W., Cheng, H.-K. & Lo, K. K.-W. Rhenium(I) polypyridine complexes functionalized with a diaminoaromatic moiety as phosphorescent sensors for nitric oxide. *New J Chem* **37**, 1711-1719 (2013).

29 Alberto, R. The Chemistry of Technetium-Water Complexes within, the Manganese Triad: Challenges and Perspectives. *Eur J Inorg Chem*, 21-31 (2009).

30 Gottschaldt, M. *et al.* Synthesis and Structure of Novel Sugar-Substituted Bipyridine Complexes of Rhenium and 99m-Technetium. *Chemistry* **13**, 10273-10280 (2007).

31 Zhang, X. & Chen, X. Preparation and characterization of 99mTc(CO)3-BPy-RGD complex as alphav beta3 integrin receptor-targeted imaging agent. *Appl Radiat Isot* **65**, 70-78 (2007).

32 Zelenka, K., Borsig, L. & Alberto, R. Metal Complex Mediated Conjugation of Peptides to Nucleus Targeting Acridine Orange: A Modular Concept for Dual-Modality Imaging Agents. *Bioconjug Chem.* **22**, 958-967 (2011).

33 Schibli, R. *et al.* Influence of the Denticity of Ligand Systems on the in Vitro and in Vivo Behavior of 99mTc(I)−Tricarbonyl Complexes: A Hint for the Future Functionalization of Biomolecules. *Bioconjug Chem.* **11**, 345-351 (2000).

34 Mundwiler, S., Kundig, M., Ortner, K. & Alberto, R. A new [2 + 1] mixed ligand concept based on [99(m)Tc(OH2)3(CO)3]+: a basic study. *Dalton Trans*, 1320-1328 (2004).

35 Probst, B., Guttentag, M., Rodenberg, A., Hamm, P. & Alberto, R. Photocatalytic H2 Production from Water with Rhenium and Cobalt Complexes. *Inorg Chem* **50**, 3404-3412 (2011).

36 Alberto, R. *et al.* A Novel Organometallic Aqua Complex of Technetium for the Labeling of Biomolecules: Synthesis of [99mTc(OH2)3(CO)3]+ from [99mTcO4]- in Aqueous Solution and Its Reaction with a Bifunctional Ligand. *J Am Chem Soc* **120**, 7987-7988 (1998).

37 Alberto, R., Ortner, K., Wheatley, N., Schibli, R. & Schubiger, A. P. Synthesis and Properties of Boranocarbonate: A Convenient in Situ CO Source for the Aqueous Preparation of [99mTc(OH2)3(CO)3]+. *J Am Chem Soc* **123**, 3135-3136 (2001).

38 Zhao, J. a., Wu, J., Hu, J., Hou, H. & Fan, Y. Syntheses, structures and magnetic properties of two new metal complexes based on a pyridyl-diphosphonate ligand. *Inorganica Chim Acta* **363**, 662-668 (2010).

39 Demoro, B. *et al.* Risedronate metal complexes potentially active against Chagas disease. *J Inorg Biochem* **104**, 1252-1258 (2010).

40 Li, C. *et al.* Synthesis, structures and surface photovoltage properties of four novel metal phosphonates with a 3D supramolecular structure. *CrystEngComm* **14**, 5479-5486 (2012).

41 Torres Martin de Rosales, R., Finucane, C., Mather, S. J. & Blower, P. J. Bifunctional bisphosphonate complexes for the diagnosis and therapy of bone metastases. *Chem Commun*, 4847-4849 (2009).

42 Zelenka, K., Borsig, L. & Alberto, R. Trifunctional Tc-99m based radiopharmaceuticals: metal-mediated conjugation of a peptide with a nucleus targeting intercalator. *Org Biomol Chem* **9**, 1071-1078 (2011).

43 Bolte, S. & Cordelieres, F. P. A guided tour into subcellular colocalization analysis in light microscopy. *J Microsc* **224**, 213-232 (2006).

44 Zhang, R. *et al.* Developing Red-Emissive Ruthenium(II) Complex-Based Luminescent Probes for Cellular Imaging. *Bioconjug Chem.* **23**, 725-733 (2012).

45 Zhang, Y. *et al.* Biophysical Studies on the Interactions of a Classic Mitochondrial Uncoupler with Bovine Serum Albumin by Spectroscopic, Isothermal Titration Calorimetric and Molecular Modeling Methods. *J Fluoresc* **21**, 475-485 (2011).

46 Devaraj, N. K. & Weissleder, R. Biomedical Applications of Tetrazine Cycloadditions. *Acc Chem Res.* **44**, 816-827 (2011).

47 Devaraj, N. K., Hilderbrand, S., Upadhyay, R., Mazitschek, R. & Weissleder, R. Bioorthogonal Turn-On Probes for Imaging Small Molecules inside Living Cells. *Angew Chem Int Ed* **49**, 2869-2872 (2010).

Chapter 3: Chlorin e6

3.1 Overview

Chlorin e6 (Ce6) (Figure 17) is a fluorescent compound that has the ability to be radiolabeled.[1,2] It can be also used as a photosensitzer for PDT offering a synthon for the creation of multi-purpose probes (optical, nuclear and PDT agents). Because porphyrins inherently accumulate in tumours[3] and have near-infrared fluorescence emission, Ce6 possesses ideal characteristics for an optical imaging agent for cancer detection. Upon incubation with cancer cells, Ce6 will localize to the mitochondria and endoplasmic reticulum, and can subsequently be imaged upon excitation with light.[4] Ce6 has been imaged successfully in vitro previously where, for example, Wawrzyńska *et al.* have imaged Ce6 in a human aortic smooth muscle cell line (T/G HA-VSMCs).[4]

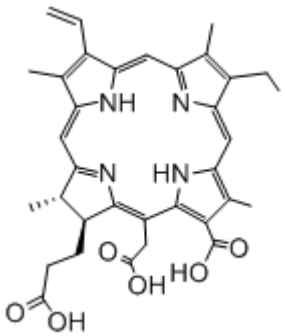

Figure 17: Structure of Chlorin e6 (Ce6).

Ce6 can be radiolabelled with technetium-99m, other radiometals and radiohalogens.[1,2] When complexed with technetium-99m or labelled with iodine-123, Ce6 will act as a nuclear imaging probe for SPECT, as well as an optical probe due to its inherent fluorescence properties. With respect to PDT, excitation with a 672 nm laser results in the generation of reactive oxygen species (ROS) which cause cytotoxic effects in cells by inducing oxidative stress, resulting in reduced function of the mitochondria and endoplasmic reticulum. This ultimately leads to programmed cell death.[4]

While Ce6 targeting is largely associated with its porphyrin nature, there are a few examples of it being targeted by specific vectors. For example, chlorin has been targeted to both folate and insulin receptors, which are both over-expressed in cancer. Li *et al.* have attached chlorin to folic acid, and saw a significant increase in uptake and phototoxicity in HeLa and Hep-2 cells (folate-receptor positive) as compared to the non-targeted chlorin.[5] Akhlyinina *et al.* synthesized BSA-insulin-Ce6 which they showed attached to insulin receptors in a human hepatoma cell line.[6]

In our work, Ce6 was attached to the PSMA inhibitor (glutamte-urea-lysine) in order to target PSMA and therefore use the multipurpose nature of Ce6 to image/treat prostate cancer. Two different constructs were initially tested: Ce6 attached directly to the PMSA inhibitor (Figure 18A) and Ce6 attached to the PSMA inhibitor through a carbon-chain linker (Figure 18B).

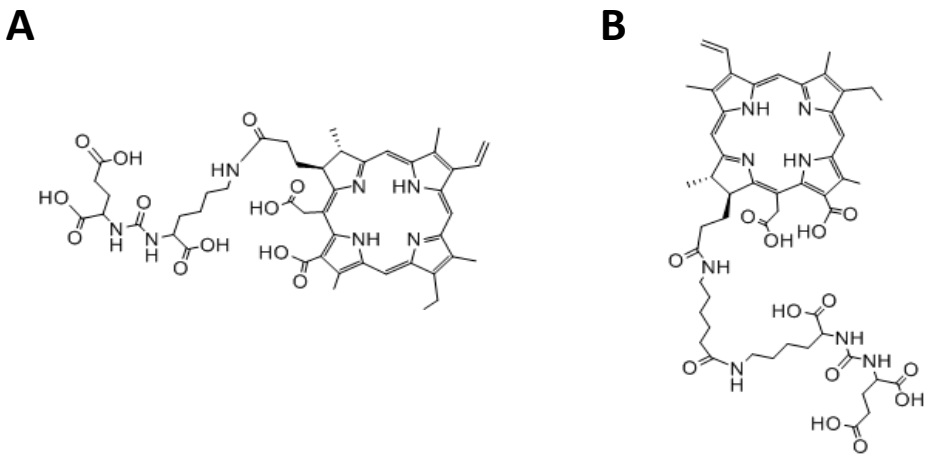

Figure 18: A) Ce6 attached directly to the PSMA inhibitor. B) Ce6 attached to the PSMA inhibitor through a carbon-chain linker.

Two additional Ce6 constructs modeled after the DNP antibody recruiting molecules (Chapter 4), have been synthesized. A polyethylene glycol (PEG) chain connects the Ce6 and glutamate-urea-lysine inhibitor. These Ce6 derivatives also contain an iodine atom, and therefore can be radiolabeled with iodine-123 for SPECT imaging (Figure 19).

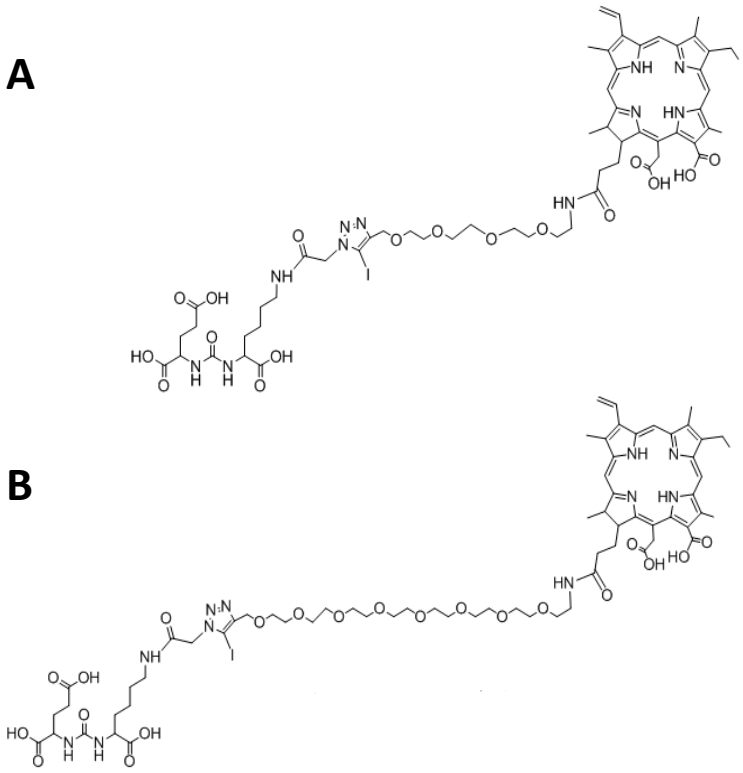

Figure 19: Iodine containing, PSMA-targeting Ce6 derivatives. A) I-Ce6 attached to the PSMA inhibitor through a PEG_4 chain. B) I-Ce6 attached to the PSMA inhibitor through a PEG_8 chain.

3.2 Synthesis and Evaluation of Chlorin-e6 Derived Inhibitors of Prostate-Specific Membrane Antigen (PSMA) for PDT of PC

The following is a manuscript on the synthesis and evaluation of the Ce6 PSMA inhibitors. My specific contribution includes the binding studies for **3-5** and **3-9** (Figure 21), all fluorescence microscopy studies, plate reader assays and flow cytometry. A radioactive binding assay was first performed to evaluate the binding affinity of the

constructs to PSMA. After confirming that the PSMA-targeted Ce6 compounds did in fact bind to PSMA, fluorescence microscopy, flow cytometry and a plate reader assay were conducted in order to assess the differential uptake of the PSMA-targeting Ce6 derivatives in a PSMA-positive and PSMA-negative cell line (LNCaP and PC3 cells, respectively).

3.3 Introduction

Prostate cancer is the most widely diagnosed disease in men, and in 2013 it is estimated that there will be 23 600 new cases of prostate cancer in Canada.[7] New therapeutic approaches and targets for prostate cancer must therefore be developed. To better treat prostate cancer, a series of new systematic and focal therapies are under development. One target that is being actively explored is prostate specific membrane antigen (PSMA), which is a type II transmembrane protein that is over-expressed on primary and malignant prostate cancers.[8] Although the role of PSMA in the prostate is not known, PSMA is being used as a target to deliver chemotherapeutics and radioisotopes.[9-13]

Because of the over expression of PSMA, it is an attractive target for photodynamic therapy (PDT). In PDT a photosensitizer (PS) is administered, and upon accumulation in cancerous tissue, light of the appropriate wavelength is applied. Absorption of light produces reactive oxygen species (ROS) which are cytotoxic to the cancer cells, and a therapeutic effect is induced.[14-16]

To determine if PSMA can be used to localize photosensitizers to prostate cancer a PDT agent was linked to glutamate-urea-lysine derived inhibitor of PSMA. Of particular interest is the porphyrin Chlorin e6 (Ce6), a photosensitizer that can also be used for diagnostic purposes. Ce6 is fluorescent, having peak fluorescence emission of 675 and 735 nm, and can therefore be used for optical imaging.[17] Additionally, Ce6 has the ability to be radiolabeled and can be used for nuclear imaging.[1,2] A Ce6 ligand capable binding PSMA could be used to localize tumours in support of biopsy and surgery and for focal PDT.

A set of PSMA-targeted Ce6 derivatives were synthesized by attaching Ce6 to the glutamate-urea-lysine derived PSMA inhibitor. The binding and uptake were evaluated in vitro to evaluate these constructs as a potential dual-purpose imaging and PDT agent for prostate cancer.

3.4 Results and Discussion

3.4.1 Chemistry. Ce6 PSMA inhibitors were prepared using literature[18-20] and novel methods by Dr. A. Genady and were fully characterized. Figure 20 shows the structure of Ce6 and the synthesized Ce6 PSMA inhibitors.

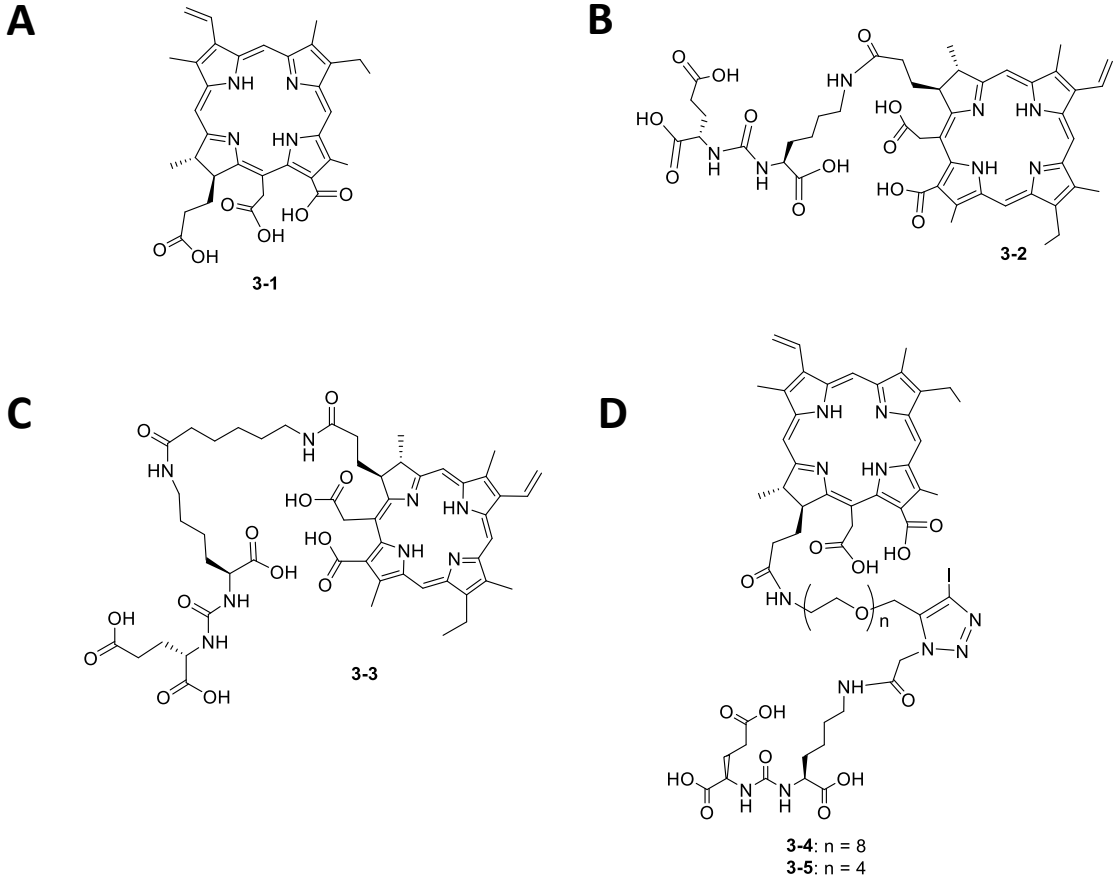

Figure 20: A) Compound **3-1**: Chlorin e6 (Ce6). B) Compound **3-2**: Ce6 attached directly to a PSMA inhibitor. C) Compound **3-3**: Ce6 attached to the PSMA inhibitor through a spacer group. D) Compounds **3-4** and **3-5**: I-Ce6 attached to the PSMA inhibitor through a PEG chain.

3.4.2 Binding Studies The binding affinities of the PSMA-targeted Chlorin e6 derivatives were assessed through use of an LNCaP cell competition binding assay (Figure 21). The triazole appending agent derived PSMA inhibitor (^{125}I-TAAG-glu-urea-lysine) was used as the radiolabeled ligand in the PSMA binding studies.[21] 2-(Phosphonomethyl)-pentanedioic acid (PMPA), a known PSMA inhibitor, was used as a positive control.[22]

Ce6 was first linked directly to the PSMA inhibitor (**3-2**), and subsequently connected through a spacer group (**3-3**). Compound **3-3** was found to have reasonable binding affinity to PSMA, exhibiting an average IC_{50} of 74 nM with respect to ^{125}I-TAAG-glu-urea-lysine. The linker between the PSMA inhibitor and Ce6 was deemed necessary as the direct attachment of Ce6 and the inhibitor gave a much poorer binding affinity (238 nM with respect to ^{125}I-TAAG-glu-urea-lysine). Due to insufficient binding of **3-2** to PSMA, this construct was not used in future studies.

It was thought that the binding affinity of the PSMA-targeted Ce6 could be increased by the addition of a polyethylene glycol (PEG) spacer between **3-1** and the PSMA inhibitor. The PEGylated derivatives were found to have the greatest binding affinities for PSMA. Compounds **3-4** and **3-5** had an average IC_{50} of 36 nM and 63 nM, respectively. After determining that **3-3**, **3-4** and **3-5** bind effectively to PSMA, further studies were performed to assess their uptake in PSMA-positive and PSMA-negative cell lines.

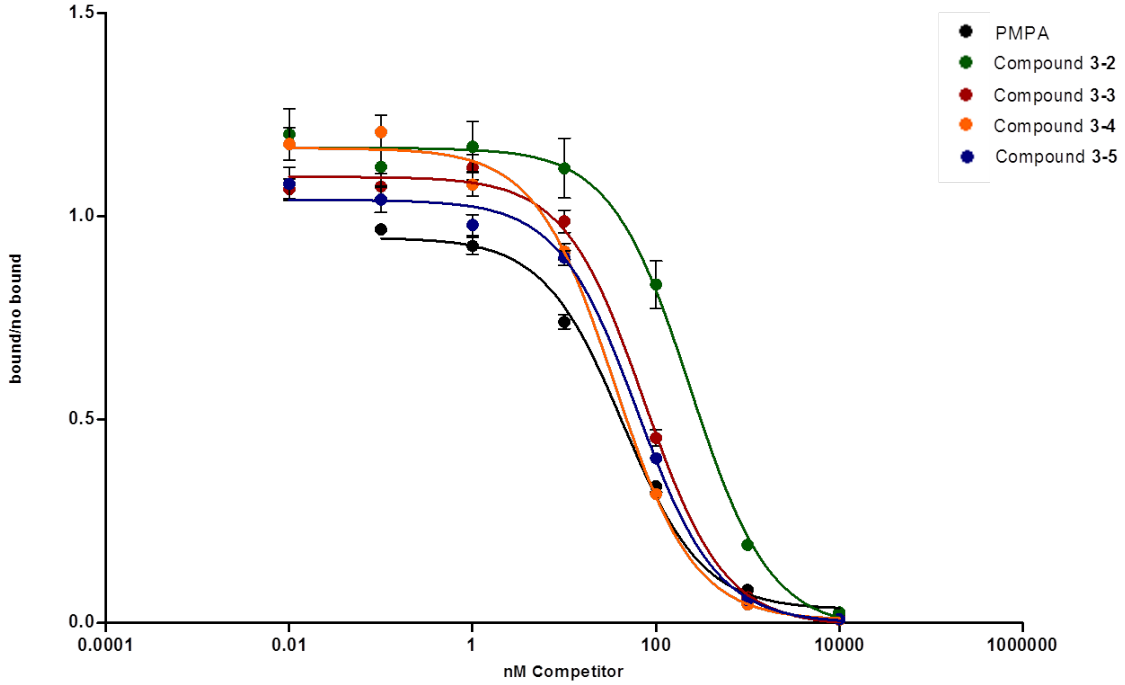

Figure 21: IC_{50} competition binding curves for the chlorin-e6 PSMA inhibitors. The curves show the combined averages from three assays (two assays for **3-2**). Average IC_{50} values for compounds **3-2**, **3-3**, **3-4** and **3-5** were 238 nM, 74 nM, 63 nM and 36 nM, respectively.

3.4.3 Cellular Uptake

Through the attachment of Ce6 to an inhibitor of PSMA, the photosensitizer can be directed specifically to malignant prostate cancer cells that express PSMA on their surface. Prior to the preparation of **3-4** and **3-5**, a study for Ce6 and **3-3** was performed with flow cytometry in order to gain quantitative information regarding uptake in LNCaP (PSMA-positive) and PC3 (PSMA-negative) cells. The cells were incubated with either 10 μM compound or vehicle (control) for 1, 4 and 6 hours and subsequently analyzed

with the Beckman Coulter Epics XL flow cytometer using the FL4 channel. Differential levels of **3-3** were observed in the LNCaP and PC3 cells. The flow cytometry data (Figure 22) shows that there is an average of 3.7 times greater uptake in LNCaP cells as compared to PC3 cells.

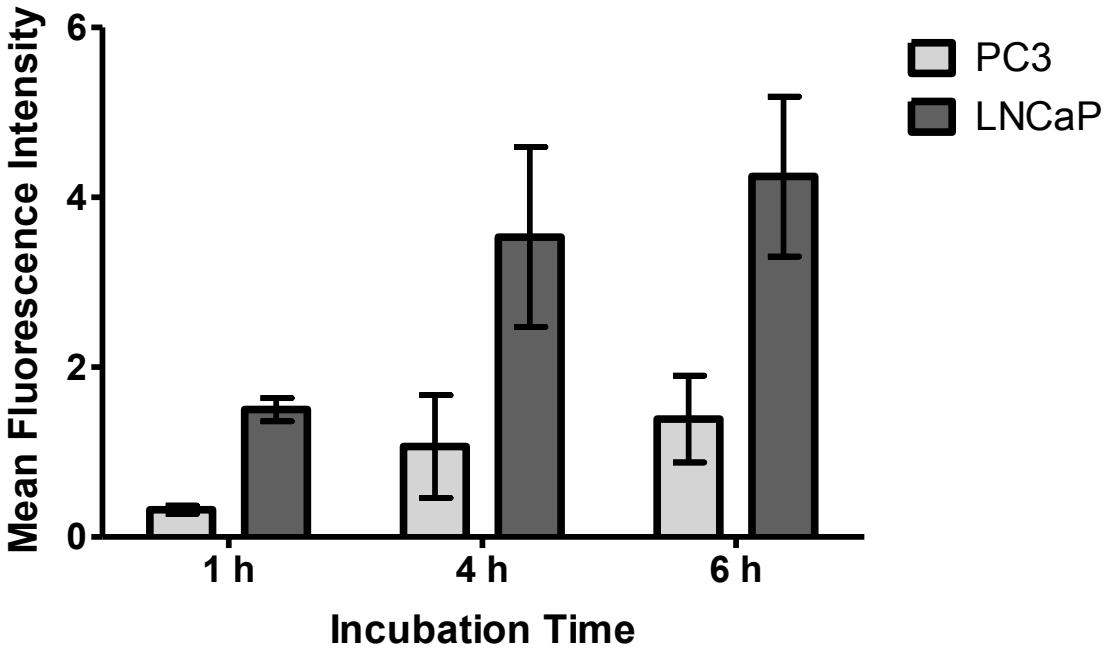

Figure 22: Flow cytometry data showing the fluorescence intensity of LNCaP cells (PSMA-positive) and PC3 cells (PSMA-negative) incubated with 10 μM of **3-3**.

A blocking study was also performed to show that uptake of **3-3** in LNCaP cells was PSMA-specific. 1 mM I-TAAG-glu-urea-lysine was co-incubated with 10 μM of **3-3** for 6 hours, resulting in a 47% decrease in fluorescence intensity of LNCaP cells as compared to the non-block experiment. PC3 cells showed no decrease in fluorescence intensity (within error) for the blocking experiment (Figure 23). The significant decrease

in mean fluorescence intensity of LNCaP cells when co-incubated with a PSMA block indicates that the increased uptake is due to PSMA binding and that it is PSMA-specific. For the PC3 cells the lack of change indicates that any uptake is due to non-specific binding and is not dependent on binding to PSMA.

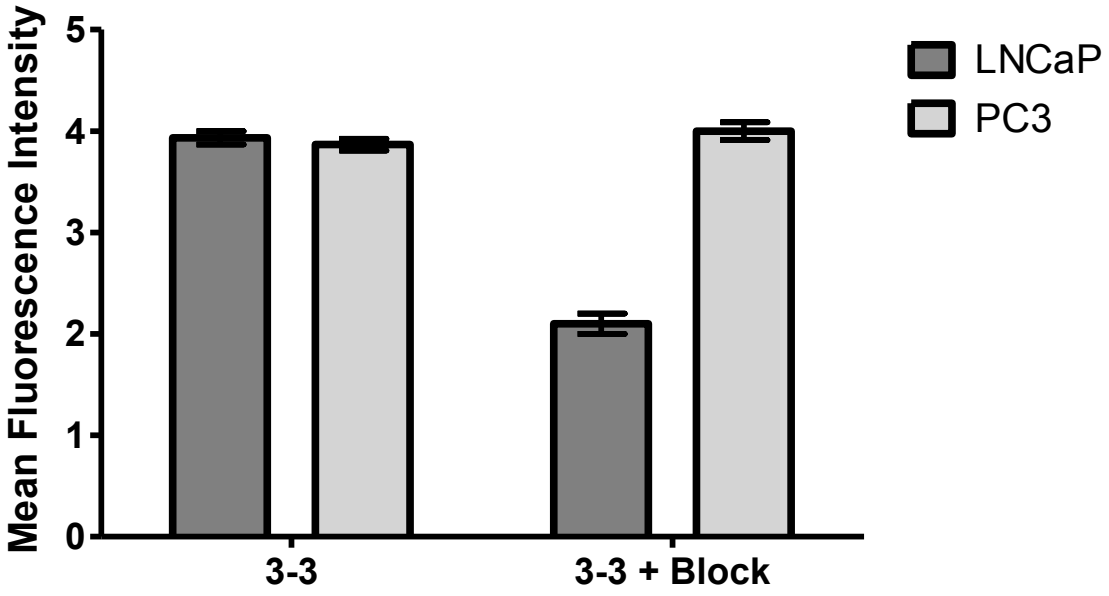

Figure 23: Flow cytometry results for a blocking experiment. 1 mM I-TAAG-glu-urea-lysine was co-incubated with 10 μM **3-3** for the blocking experiment.

A comparison of mean fluorescence intensities for LNCaP cells incubated with either non-targeted Ce6 (**3-1**) or PSMA-targeted Ce6 (**3-3**) at 1, 4 and 6 h were made (Figure 24). As shown, there was much greater uptake of **3-1** in comparison to **3-3** at all time points, with the 6 hour time point showing the fluorescence intensity from incubation with **3-1** to be 26.5 times greater than that from incubation with **3-3**.

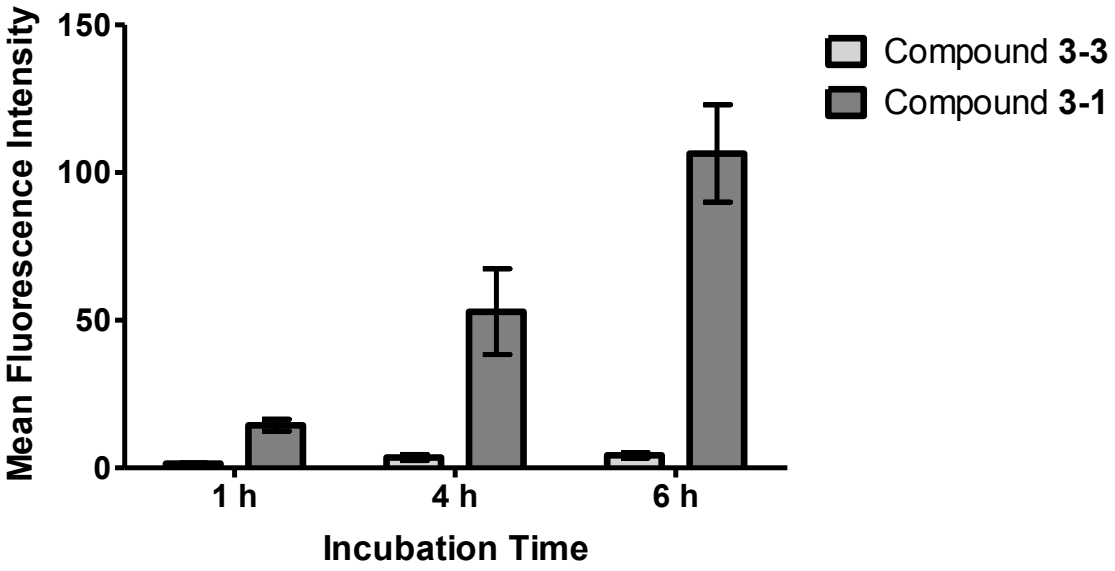

Figure 24: Fluorescence intensity of LNCaP cells incubated with either 10 μM **3-1** (non-targeted Ce6) or **3-3**.

With the goal of further increasing the uptake in a PSMA-positive cell line, a new class of PSMA inhibitors containing Ce6 were prepared. After determining sufficient binding affinity to PSMA for **3-4** and **3-5**, a plate reader assay was performed in order to establish the differential uptake of the PSMA-targeted Ce6 compounds in a PSMA-positive and PSMA-negative cell line (LNCaP and PC3 cells, respectively). 10 μM solutions of **3-1**, **3-3**, **3-4** and **3-5** were prepared and incubated with LNCaP and PC3 cells for 6 hours at 37˚C. The fluorescence intensity of the cells were measured with a plate reader, and normalized to protein content (Figure 25).

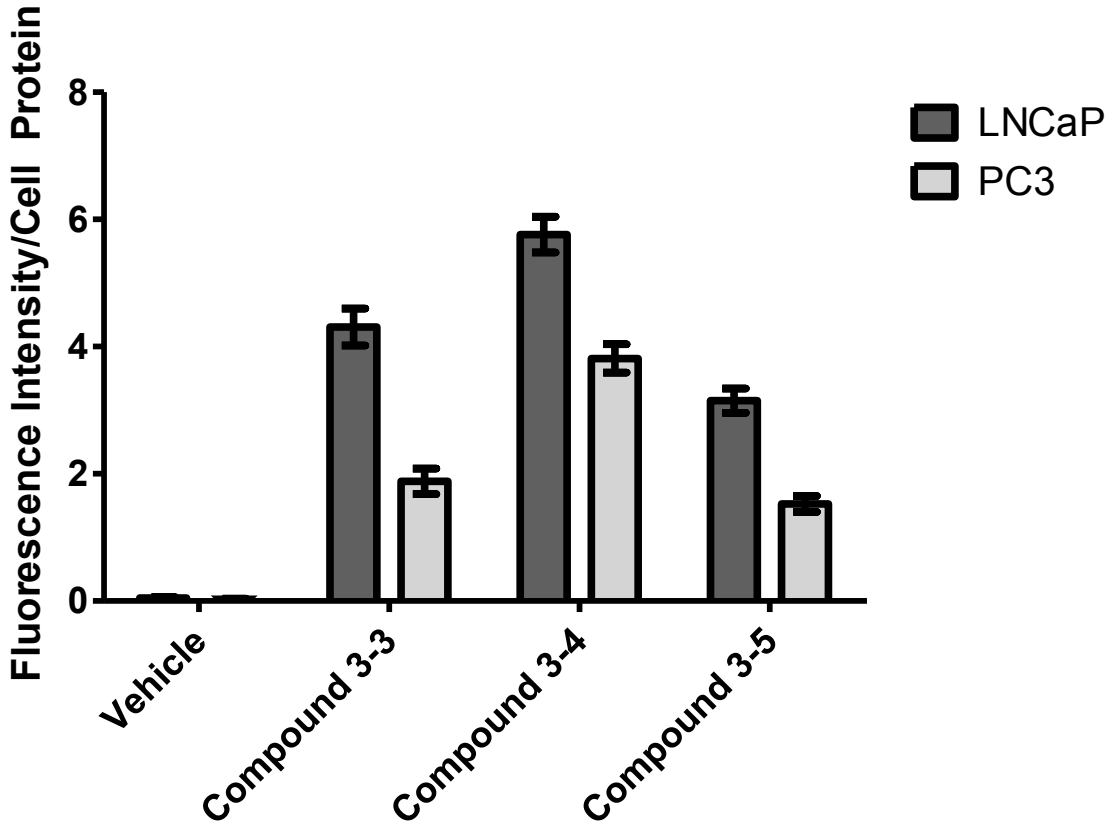

Figure 25: LNCaP and PC3 cells were incubated with 10 μM of the appropriate Ce6 derivative for 6 h. Fluorescence intensity normalized to cell protein was significantly greater in LNCaP cells as compared to PC3 cells.

It was expected that LNCaP cells would have greater fluorescence intensity than PC3 cells because the former have higher expression of PSMA. This was the case as seen for all three PSMA-targeted constructs tested, and is in agreement with the flow cytometry data for **3-3**. Compound **3-4** exhibited the greatest fluorescence intensity in LNCaP cells of the PSMA-targeted Ce6 derivatives. However, the difference between LNCaP cell and PC3 cell fluorescence intensity appeared to be the lowest for **3-4** (percent difference =

41%), with **3-3** showing the greatest difference between the PSMA-positive and PSMA-negative cell line (percent difference = 78%).

As a means of comparison, the cells were also incubated with **3-1**. Ce6 enters the cell through both passive diffusion and endocytosis, specifically, LDL-mediated endocytosis.[23] The mitochondria and endoplasmic reticulum have shown to be sites of localisation of Ce6 in cells.[4] The amount of **3-1** taken up was comparable for both LNCaP and PC3 cells (percent difference = 8%), with fluorescence intensity values much greater than that for their PSMA-targeted analogues. Although both cell lines exhibited much greater fluorescence levels, we were not able to discern between the PSMA-positive and PSMA-negative cell line, as we could for incubation with **3-3**, **3-4** and **3-5**. Being able to distinguish between the fluorescence of the PSMA-positive and PSMA-negative cell line is of upmost importance as it represents being able to distinguish between cancerous tissue (PSMA-positive) and normal prostate tissue in vivo.

Fluorescence microscopy was used to visualize the uptake of the PSMA-targeted Ce6 analogues in LNCaP and PC3 cells. LNCaP and PC3 cells were plated on cover slides, and incubated with 10 μM of either **3-1**, **3-3**, **3-4**, **3-5**, or the equivalent amount of vehicle, for a three hour period. The cells were visualized with fluorescence microscopy, and it was observed that LNCaP cells incubated with **3-3**, **3-4**, or **3-5**, were distinguishably brighter than their PC3 counterparts (Figure 26). This is consistent with both the plate reader assay and flow cytometry studies.

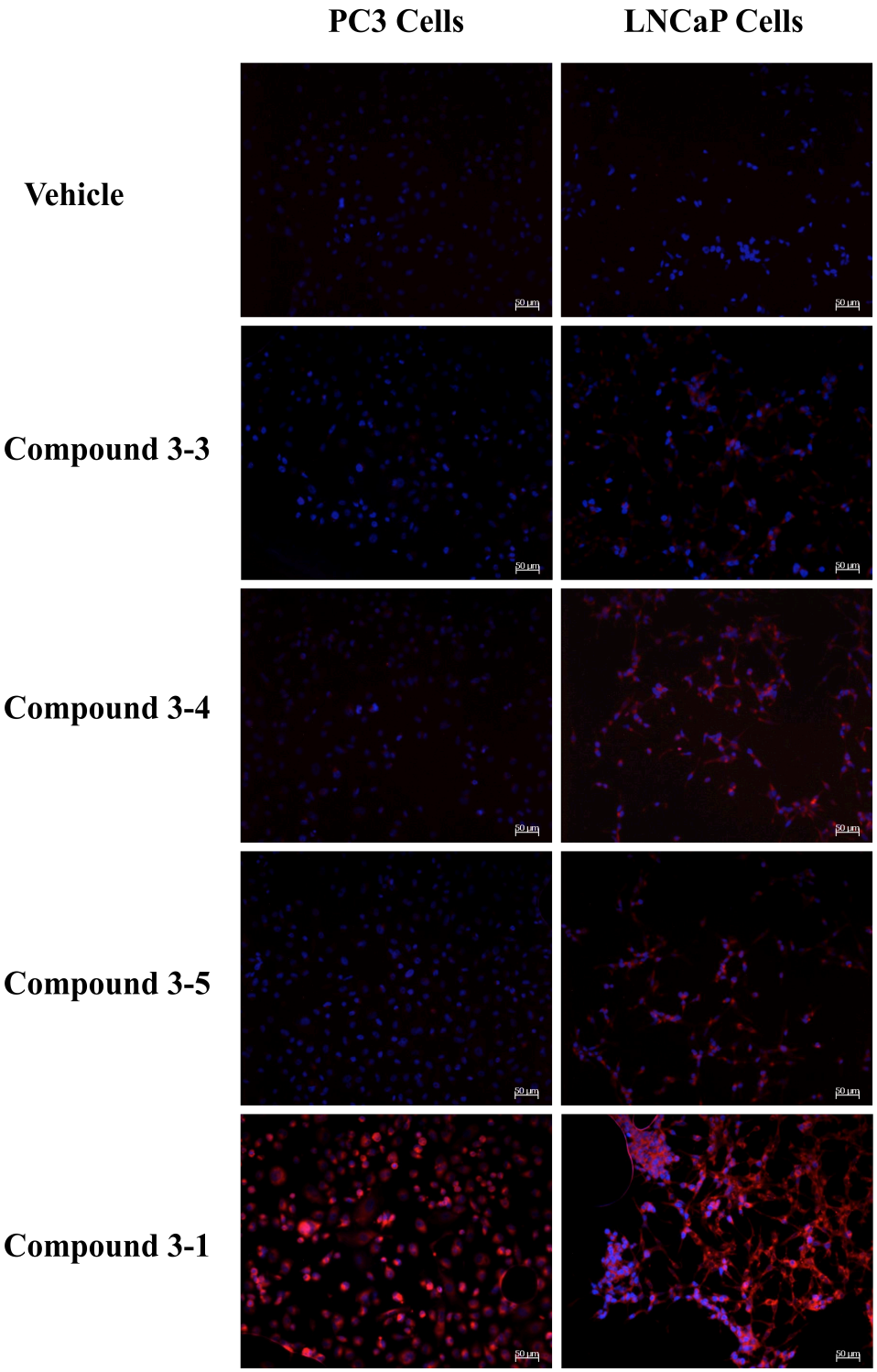

Figure 26: Fluorescence microscopy images of PC3 and LNCaP cells incubated with Ce6 and compounds **3-3**, **3-4**, and **3-5**.

3.5 Conclusion

A ligand binding study was conducted to determine the affinities of a series of different PSMA-targeted Ce6 compounds to PSMA. Compound **3-3** had sufficiently high binding affinity to PSMA (74 nM) to warrant further testing. Flow cytometry and fluorescence microscopy showed differential uptake of **3-3** in PSMA-positive and PSMA-negative cell lines, with LNCaP cells exhibiting an average of four times greater fluorescence intensity than PC3 cells. Uptake was low in comparison to Ce6 alone, which in contrast showed poor selectivity between PSMA-positive and PSMA-negative cell lines. Selectivity however is of upmost importance because by directing the photosensitizer to PSMA exhibiting cells, non-cancerous cells can be spared any cytotoxic effects induced by PDT.[24]

A second class of compounds (**3-4** and **3-5**), containing a new triazole linker were synthesized in an effort to increase uptake in the PSMA-positive cell line. These Ce6 PSMA inhibitors were found to have a lower IC_{50} than **3-3** (36 and 63 nM for **3-4** and **3-5**, respectively), but a plate reader assay and fluorescence microscopy showed little increase in uptake. Furthermore, the plate reader assay showed **3-3** had the greatest difference in uptake between the PSMA-positive and PSMA-negative cell line.

3.6 Experimental Section

Cells and Materials LNCaP cells (ATCC no. CRL-1740) were cultured in RPMI 1640 media supplemented with 10% fetal bovine serum, 2 mM L-glutamine, 1 mM sodium pyruvate, 10 mM HEPES, 1% penicillin streptomycin and 0.25% D-glucose. The cell line was maintained at 37 °C and 5% CO_2. Binding buffer for the assays consisted of RPMI 1640 media supplemented with 0.5% bovine serum albumin. RIPA buffer, also prepared for binding studies, contained 100 mM Tris pH 8, 50 mM NaCl, 1% NP40, 0.5% Na deoxycholate and 0.1% SDS. HEPES buffered saline consisted of 100 mM HEPES, 120 mM NaCl, 1.2 mM $MgSO_4$, 5mM KCl, 15 mM sodium acetate and 10 mM D-glucose.

LNCaP Cell Competition Binding Assay LNCaP cells were plated in 24-well plates at either 2.1×10^5 cells/well (for a 2-day plating), or 1.6×10^5 cells/well (for a 3-day plating). A solution of ^{125}I-TAAG-glutamate-urea-lysine (1 nM, 37 kBq/mL) in binding buffer (RPMI 1640 and 0.5% BSA) was prepared. Varying concentrations (0, 0.01, 0.1, 1, 10, 100, 1000 and 10000 nM) of the competing Chlorin-e6 derivative (**3-2**, **3-3**, **3-4** or **3-5**) in the binding buffer containing ^{125}I-TAAG-glutamate-urea-lysine were prepared. 300 µL of each of the competitor concentrations were added to individual wells, and incubated at room temperature for 1 h, and samples were prepared in triplicate. After incubation, cells were harvested and washed three times with binding buffer. The cells were then lysed by incubating at 37 °C in 500 µL RIPA buffer for 30 min. 400 µL of the RIPA solution containing the cells were then transferred and counted using an automated gamma counter for 10 minutes. As a positive control, the assay was concurrently

performed with 2-(phosphonomethyl)-pentanedioic acid (PMPA), which is a known PMSA inhibitor.[22] Competitive binding curves and IC_{50} values were generated and data analyzed using GraphPad Prism 5 (GraphPad Software, Inc.).

Flow Cytometry: LNCaP and PC3 cells were plated at a density of 5.0 x 10^5 cells/well (in a 6-well plate) and incubated for 2 days at 37˚C and 5% CO_2. Following the 2 day incubation period, the media was removed by aspiration, and the wells were washed with HEPES buffered saline. For each cell line, 1.5 mL of either 10 μM **3-1** or **3-3**, or the equivalent amount of vehicle, was added to the wells in triplicate. The cells were incubated at 37˚C and 5% CO_2 for 1, 4 or 6 h. Following incubation the solutions were removed by aspiration and the cells were removed by adding 0.5 mL of cell dissociation solution (Sigma) to each of the wells, and incubating at 37˚C and 5% CO_2 until the cells detached from the surface. The cells were harvested and transferred to labelled Eppendorf tubes, where they were washed three times with PBS. A Beckman Coulter Epics XL flow cytometer using the FL4 channel was used to quantify the fluorescence from all samples of cells.

Blocking Experiment: LNCaP and PC3 cells were plated at a density of 4.0 x 10^5 cells/well (in a 12-well plate) and incubated for 2 days at 37˚C and 5% CO_2. Following the 2 day incubation period, the media was removed by aspiration, and the wells were washed with HEPES buffered saline. For each LNCaP and PC3 cells, 1.5 mL of the 10 μM solution of **3-3** was added to three wells. To the remaining three wells a 1.5 mL solution consisting of 10 μM **3-3** and 1 mM I-TAAG-glu-urea-lysine in HEPES buffered

saline was added. The cells were incubated with these solutions for 6 h at 37˚C after which the solutions were removed and cells detached using a cell dissociation solution (Sigma). The cells were then washed three times with PBS and flow cytometry was performed using the Beckman Coulter Epics XL flow cytometer and the FL4 channel.

Fluorescence Assay LNCaP cells and PC3 cells were plated in a 24-well plate at a density of 1.6×10^5cells/well. Following a 3-day incubation at 37˚C and 5% CO_2, the cells were washed once with HEPES buffered saline. In triplicate, 1.5 mL of 10 μM solutions of either **3-1**, **3-3**, **3-4**, **3-5**, or the equivalent amount of vehicle was added to the appropriate wells. The cells were incubated at 37˚C for 6 h. Following incubation, the solutions were removed, and 100 μL of cell dissociation solution (Sigma) was added and the cells were left to incubate at 37˚C for 10 min. To each well, 500 μL of PBS was added, and the cells were transferred to appropriately labeled tubes. The cells were washed a total of three times with PBS, and 150 μL of 1% Triton-X lysing solution added. The cells were left to incubate at 37˚C for an additional 30 minutes. Fluorescence intensity was measured on a Tecan Infinite M1000 plate reader by exciting at 400 nm and detecting at 660 nm. A Pierce BCA Protein Assay was also performed, and fluorescence intensity values were normalized to the protein content in each sample.

Cell Imaging LNCaP cells and PC3 cells were plated on cover glasses placed inside a 6-well plate with a density of 5.0×10^5 cells/well. The cells were left to incubate at 37˚C and 5% CO_2 for 2 days. Following the incubation, the cover glasses were washed once with HEPES buffered saline and transferred to individual wells in a 12-well plate. To

each well 1.5 mL of the appropriate 10 μM solution of either **3-1**, **3-3**, **3-4**, **3-5**, or the equivalent amount of vehicle was added. The cells were then incubated for 3 h at 37˚C. Following the incubation, the solutions were removed and the cells were washed three times with PBS. To each well, 1.5 mL of 4% paraformaldehyde (PFA) was added, and the samples were left to incubate at room temperature for 10 min. The 4% PFA was removed and the cells were washed an additional 3 times with PBS. The cover glasses were the mounted onto slides using ProLong Gold Antifade Reagent with DAPI (Invitrogen). The cells were imaged using the Zeiss Axioplan 2 microscope with a DAPI and a special Cy5 filter cube.

3.7 References

1 Babbar, A. K., Singh, A. K., Goel, H. C., Chauhan, U. P. S. & Sharma, R. K. Evaluation of Tc-99m-labeled photosan-3, a hematoporphyrin derivative, as a potential radiopharmaceutical for tumor scintigraphy. *Nucl Med Biol* **27**, 587-592 (2000).

2 Yang, S.-G. *et al.* (99)mTc-hematoporphyrin linked albumin nanoparticles for lung cancer targeted photodynamic therapy and imaging. *J Mater Chem* **20**, 9042-9046 (2010).

3 Chin, W. W. L. *et al.* In-vivo optical detection of cancer using chlorin e6--polyvinylpyrrolidone induced fluorescence imaging and spectroscopy. *BMC Med Imaging.* **9**, 1-1 (2009).

4 Wawrzynska, M. *et al.* In Vitro Photodynamic Therapy with Chlorin e6 Leads to Apoptosis of Human Vascular Smooth Muscle Cells. *Arch Immunol Ther Exp* **58**, 67-75 (2010).

5 Li, D. *et al.* A novel chlorin-PEG-folate conjugate with higher water solubility, lower cytotoxicity, better tumor targeting and photodynamic activity. *J Photochem Photobiol B* **9**, 28-37 (2013).

6 Akhlynina, T. V., Rosenkranz, A. A., Jans, D. A. & Sobolev, A. S. Insulin-mediated intracellular targeting enhances the photodynamic activity of chlorin e6. *Cancer Res* **55**, 1014-1019 (1995).

7 Siegel, R., Naishadham, D. & Jemal, A. Cancer statistics, 2013. *CA Cancer J Clin* **63**, 11-30 (2013).

8 Chang, S. S. *et al.* Prostate-specific membrane antigen is produced in tumor-associated neovasculature. *Clin Cancer Res* **5**, 2674-2681 (1999).

9 Farokhzad, O. C. *et al.* Targeted nanoparticle-aptamer bioconjugates for cancer chemotherapy in vivo. *Proc Natl Acad Sci U S A* **103**, 6315-6320 (2006).

10 Dhar, S., Gu, F. X., Langer, R., Farokhzad, O. C. & Lippard, S. J. Targeted delivery of cisplatin to prostate cancer cells by aptamer functionalized Pt(IV) prodrug-PLGA-PEG nanoparticles. *Proc Natl Acad Sci U S A* **105**, 17356-17361 (2008).

11 Henry, M. D. *et al.* A prostate-specific membrane antigen-targeted monoclonal antibody-chemotherapeutic conjugate designed for the treatment of prostate cancer. *Cancer Res* **64**, 7995-8001 (2004).

12 Hillier, S. *et al.* [131I]MIP-1466, a small molecule prostate-specific membrane antigen (PSMA) inhibitor for targeted radiotherapy of prostate cancer (PCa). *J Nucl Med Meeting Abstracts* **53**, 170- (2012).

13 Hillier, S. *et al.* [131I]MIP-1375, a small molecule prostate-specific membrane antigen (PSMA) inhibitor for targeted therapy of prostate cancer (PCa). *J Nucl Med Meeting Abstracts* **52**, 361- (2011).

14 Dolmans, D. E. J. G. J., Fukumura, D. & Jain, R. K. Photodynamic therapy for cancer. *Nat Rev Cancer* **3**, 380-387 (2003).

15 Liu, T., Wu, L. Y., Choi, J. K. & Berkman, C. E. Targeted photodynamic therapy for prostate cancer: inducing apoptosis via activation of the caspase-8/-3 cascade pathway. *Int J Oncol* **36**, 777-784 (2010).

16 Chen, Q. *et al.* Preclinical Studies in Normal Canine Prostate of a Novel Palladium-Bacteriopheophorbide (WST09) Photosensitizer for Photodynamic Therapy of Prostate Cancer. *Photochem Photobiol* **76**, 438-445 (2002).

17 Spikes, J. D. New trends in photobiology: Chlorins as photosensitizers in biology and medicine. *J Photochem Photobiol B* **6**, 259-274 (1990).

18 Maresca, K. P. *et al.* A Series of Halogenated Heterodimeric Inhibitors of Prostate Specific Membrane Antigen (PSMA) as Radiolabeled Probes for Targeting Prostate Cancer. *J Med Chem* **52**, 347-357 (2008).

19 Postma, R. & Schröder, F. H. Screening for prostate cancer. *Eur J Cancer* **41**, 825-833 (2005).

20 Murelli, R. P., Zhang, A. X., Michel, J., Jorgensen, W. L. & Spiegel, D. A. Chemical Control over Immune Recognition: A Class of Antibody-Recruiting Small Molecules That Target Prostate Cancer. *J Am Chem Soc* **131**, 17090-17092 (2009).

21 Darwish, A. *et al.* Triazole Appending Agent (TAAG): A New Synthon for Preparing Iodine-Based Molecular Imaging and Radiotherapy Agents. *ACS Med Chem Lett.* **3**, 313-316 (2012).

22 Jackson, P. F. *et al.* Design, synthesis, and biological activity of a potent inhibitor of the neuropeptidase N-acetylated alpha-linked acidic dipeptidase. *J Med Chem* **39**, 619-622 (1996).

23 Mojzisova, H., Bonneau, S., Vever-Bizet, C. & Brault, D. Cellular uptake and subcellular distribution of chlorin e6 as functions of pH and interactions with membranes and lipoproteins. *Biochimica Et Biophysica Acta-Biomembranes* **1768**, 2748-2756 (2007).

24 Liu, T., Wu, L. Y., Choi, J. K. & Berkman, C. E. In Vitro Targeted Photodynamic Therapy With a Pyropheophorbide-a Conjugated Inhibitor of Prostate-Specific Membrane Antigen. *Prostate* **69**, 585-594 (2009).

Chapter 4: Probes for Combining Antibody Recruitment and Molecular Imaging and Therapy

4.1 Introduction

As noted in Chapter 1, Murelli *et al.* have developed antibody-recruiting small molecules (ARM-Ps) for treating prostate cancer by inducing an immune response. The ARM-P is comprised of a targeting group (cell binding terminus - CBT) that binds to the cell type of interest, and an antibody terminus (ABT), which recruits the immune response. The CBT in this case is a PSMA inhibitor for targeting PSMA present on prostate cancer cells. The ABT of the ARM-P is 2,4-dinitrophenyl (DNP) group, which recruits anti-DNP antibodies. The endogenous anti-DNP is comprised of 0.8% of IgG and 1.0% of IgM circulating in the human body.[1]

Murelli *et al.* assessed their ARM-Ps for antibody recruitment with flow cytometry and fluorescence microscopy by utilizing Alexa Fluor 488 conjugated anti-DNP. Through flow cytometry they found that the spacing between the glu-urea-lysine derived PSMA inhibitor and the DNP required at least 8 oxyethylene units in order to maximize anti-DNP binding to compound **4-1** (Figure 27). They were able to visualize binding of Alexa Fluor 488 conjugated anti-DNP to the ARM-P bound to LNCaP cells through fluorescence microscopy, and showed specificity through a blocking study with 2-PMPA.

Lastly, they showed that the ARM-P was able to induce a cytotoxic effect on LNCaP cells in vitro.[1]

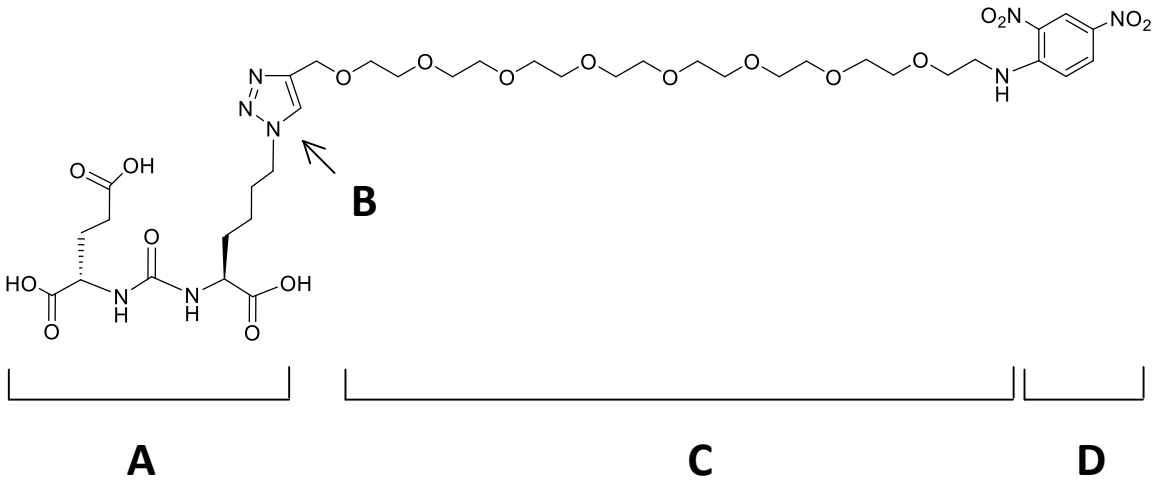

Figure 27: Compound **4-1** A) PSMA binding group B) Triazole linker. C) Spacer D) DNP antibody recruiting group

The Valliant group has adapted the ARM-P (compound **4-1**) developed by Murelli *et al.* to include the addition of iodine, which allows for the construct to be labelled with ^{131}I or ^{123}I. When radiolabeled with ^{131}I, the construct acts as a dual-therapeutic agent, through its ability to behave as both a radiopharmaceutical and to induce an immune response. When radiolabeled with ^{123}I, the construct acts as a SPECT agent, thereby allowing for treatment monitoring during antibody recruitment therapy.

Different iodine-containing derivatives were developed, and their binding affinities were assessed using an LNCaP radioactive binding assay. The derivative with the best binding affinity (IC_{50} of 3 nM with respect to ^{125}I-TAAG-glu-urea-lysine) did not have a PEG

chain connecting the glu-urea-lysine inhibitor and the DNP (compound **4-2**). The derivative containing a PEG chain between the PSMA inhibitor and DNP that had the best binding affinity (IC_{50} of 14 nM with respect to ^{125}I-TAAG-glu-urea-lysine) was compound **4-3** (Figure 28).

A

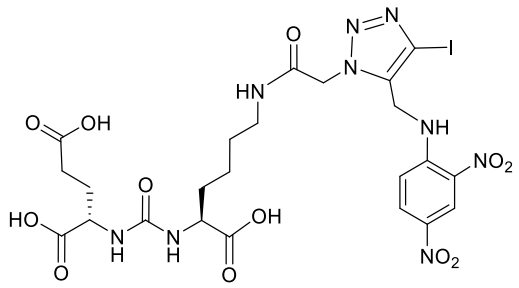

4-2

B

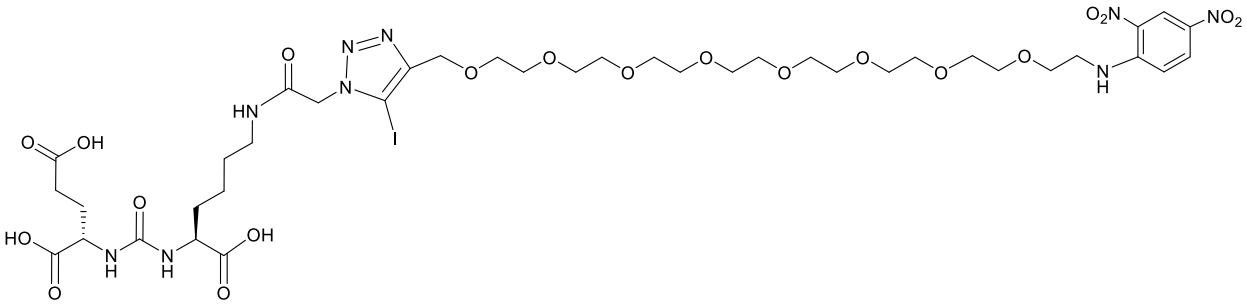

4-3

Figure 28: The iodine containing PSMA-targeting antibody recruiting construct contains the glu-urea-lysine PSMA-inhibitor on one end, and the anti-body recruiting 2,4-dinitrophenyl (DNP) on the other. A) compound **4-2** B) compound **4-3**

After screening of the iodine containing, PSMA-targeting, antibody recruiting small molecules, binding to the target and ability to recruit antibodies were assessed and compared to that of the ARM-P developed by Murelli *et al.* Confirming in vitro that antibody recruitment occurs is the key step in testing the potential utility of combined radio-immunotherapy.

4.2 Results

Fluorescence Assay

Both flow cytometry and a plate reader were used to assess the fluorescence intensity of the assay samples. The ARM-P8 (**4-1**) developed by Murelli *et al.* was used as a positive control against the iodinated versions developed by the Valliant group (compounds **4-2** and **4-3**). For compound **4-3**, flow cytometry data indicated that the iodinated compound appears to bind the target and recruit antibodies with slightly more efficiency than the non-iodinated compound (Figure 29). This is in agreement with the PSMA binding competition screening results for the compounds, which gave an average IC_{50} of 24 nM and 14 nM with respect to ^{125}I-TAAG-glu-urea-lysine, for compounds **4-1** and **4-3**, respectively.

When the PSMA targets were blocked with the addition of excess 2-PMPA, binding of anti-DNP was significantly diminished. This shows that binding of **4-3** to the LNCaP cells was PSMA-specific. Therefore, PSMA-positive cells should have increased

recruitment of antibodies, meaning an increased immune response, and thus selective cell death of the cancer cells.

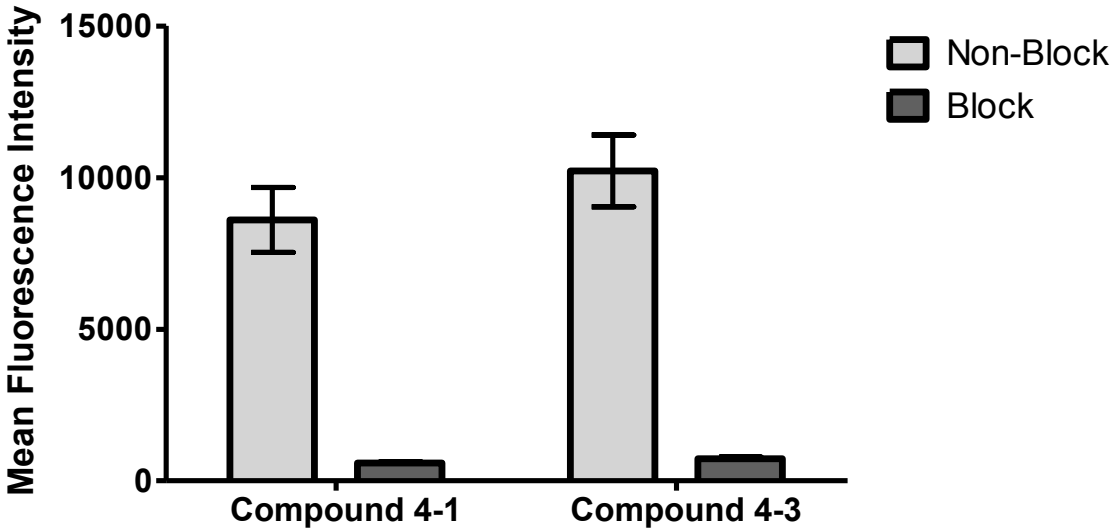

Figure 29: Flow cytometry results: LNCaP cells were incubated with 50 nM of the antibody recruiting molecule, along with Alexa Fluor 488 anti-DNP (non-block). PMPA was additionally added for 'block' samples.

The fluorescence intensity values of the samples were also measured with the plate reader. The plate reader showed similar results in that the samples blocked with PMPA had a reduced fluorescence intensity in comparison to the non-blocked samples (Figure 30). As found with the flow cytometry data, LNCaP cells incubated with **4-3** had a slightly higher fluorescence intensity than that for cells incubated with **4-1** (percent difference = 14%), most likely due to the increased binding affinity to PSMA.

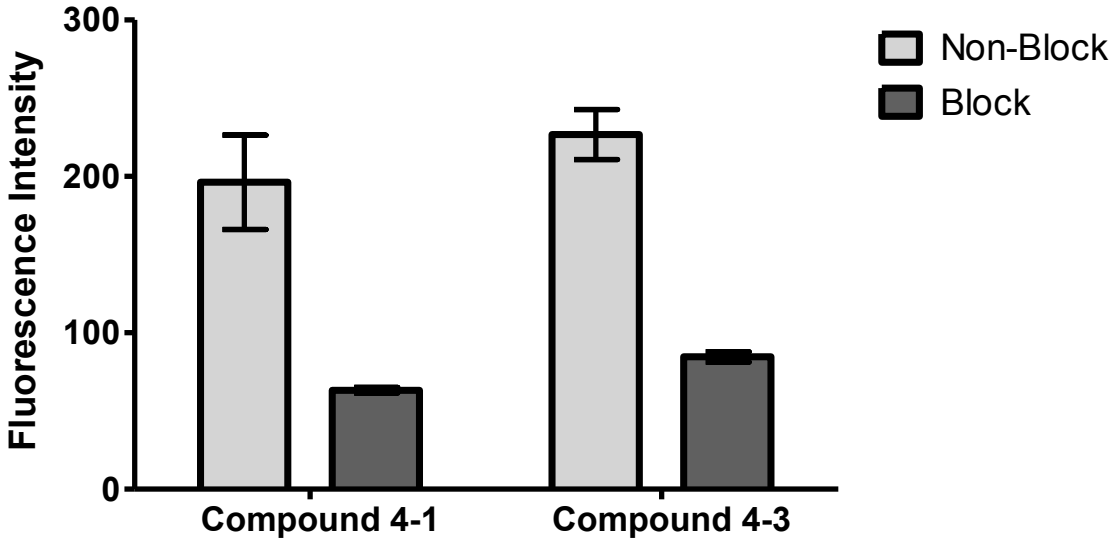

Figure 30: Plate reader fluorescence intensity results. LNCaP cells were incubated with 50 nM of either **4-1** or **4-3** alongside AlexaFluor 488 anti-DNP and either PMPA (block) or the equivalent volume of vehicle.

The assay was also performed for compound **4-2**, which had a direct attachment between the PSMA inhibitor and the DNP (Figure 31). Once again, the assay was repeated alongside **4-1**, which acted as a positive control. Compound **4-2** was found to have the best binding affinity for PSMA of all derivatives tested (IC_{50} of 3 nM with respect to ^{125}I-TAAG-glu-urea-lysine). Although the binding affinity to PSMA was high, we speculated that recruitment of anti-DNP may be diminished with this compound because DNP is located so close to the binding site, thereby hindering the antibody-hapten interaction.

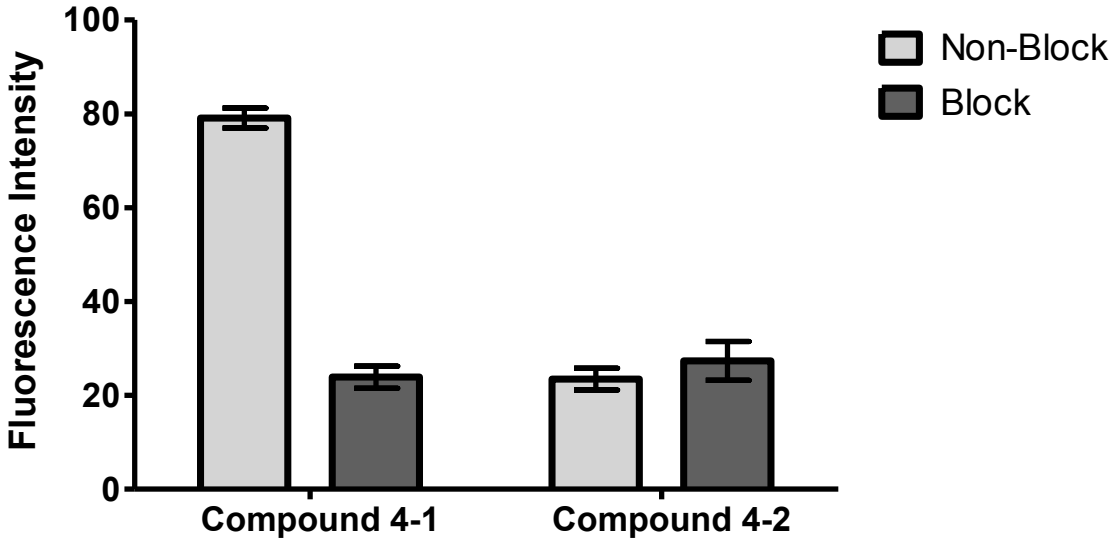

Figure 31: Plate reader fluorescence intensity results. LNCaP cells were incubated with either **4-1** (positive control) or **4-2**, alongside Alexa Fluor 488 anti-DNP. PMPA was also added as a block for 'block' samples.

As seen in Figure 31, no significant difference in fluorescence intensity was observed for cells incubated with **4-2** with and without excess PMPA. The positive control (compound **4-1**) showed a significant decrease in fluorescence intensity when PSMA sites were blocked with PMPA. This indicates **4-1** is binding to PSMA and recruiting the fluorescent anti-DNP. Although in the case of **4-2** the compound may be binding to PSMA, the fluorescently labeled anti-DNP is not being recruited to the cells as demonstrated by the relatively low level of fluorescence intensity for non-block samples.

4.3 Conclusion and Future Work

Confirmation of target binding and antibody recruitment to a PSMA positive cell line was confirmed for compound **4-3**. Compound **4-2** had the greatest binding affinity to PSMA, having an IC_{50} of 3 nM, but was unable to recruit anti-DNP antibodies to the site. LNCaP cells incubated with **4-3** and Alexa Fluor 488 anti-DNP (non-block samples) had the greatest fluorescence intensity due to its superior ability to recruit anti-DNP. This coincides with **4-3** having a slightly lower IC_{50} than **4-1**. Confirmation that anti-DNP is in fact recruited specifically to a PSMA-positive cell line indicates that **4-3** can be used to assess the benefit of combining radiotherapy and immunotherapy. This construct therefore represents the first class of small molecule probes that can be used for imaging and both radiotherapy and immunotherapy.

In order to validate the dual-therapeutic effect of these compounds, the radiotherapy aspect of the probe needs to be tested. A preclinical radiotherapeutic study would involve administering a dose of **4-3** radiolabeled with ^{131}I, and taking tumour measurements in the weeks following to determine whether there is a therapeutic effect. In vivo radiotherapeutic studies have been performed with both ^{131}I labelled PSMA-inhibiting small molecules or antibodies. Vallabhajosula and coworkers have labelled the PSMA-binding antibody J591 with ^{131}I, and examined the therapeutic ability by monitoring tumour growth inhibition in nude mice bearing LNCaP xenografts. A single dose (3.7 and 11.1 MBq) of the radiotherapeutic was injected, and tumour size was monitored. The mice that received the 3.7 MBq injection showed no significant reduction in tumour size. The group that received the 11.1 MBq injection however saw a tumour size reduction of

75% over the 35-40 day period, although 40% of the mice injected in this group died within 10 days of being injected.[2]

Hillier *et al.* developed [^{131}I]MIP-1466, a small molecule that binds to PSMA. They injected mice with either 1.9, 5.6 or 16.7 MBq and tumour growth and weight measurements were taken twice weekly. In order to show that binding was specific, 10 mg/kg of PMPA was also injected alongside the radioactive compound in a group of mice. Tumour doubling times increased with increasing dose (55, 89 and >130 days for the 1.9, 5.6 and 16.7 MBq groups), and those also injected with PMPA had a tumour doubling time similar to the control of 16 days.[3]

4-3 can be radiolabeled with ^{131}I, and a maximum tolerated dose (MTD) study can be performed in order to determine the greatest quantity of activity that can be injected into the mouse without causing death or weight loss below 20%. Mice will be injected with the following doses: 1.9, 5, 15 and 35 MBq. Tumour and weight measurements should be taken over a period of 21 days. After determining the MTD further radiotherapy studies could be performed with this dose and a larger group of mice.

After confirming the radiotherapeutic effect on the tumour induced by the ^{131}I compound, the study could be expanded to test the immunotherapy aspect of this class of compounds. Dubrovska *et al*. have demonstrated antibody recruitment therapy in vivo using a prostate cancer model. LNCaP (PSMA-positive) and DU145 (PSMA-negative) tumours were grown, and mice were immunized with DNP-KLH and injected with peripheral blood mononuclear cells. Once tumours had grown, injection with the PSMA-targeted antibody

recruiting small molecules occurred three times per week over a two week period. Tumours were measured and growth as a measure of volume was inhibited 4.8-fold in LNCaP tumours as compared to the control. No significant difference in tumour growth was found as compared to the control for DU145 tumours.[4]

This study can be adapted for our iodine-containing antibody recruiting small molecules. Cold **4-3** can be injected in mice containing LNCaP tumours and tumour growth will be compared to that of a control. After confirming that this class of compounds can slow tumour growth by both radiotherapy and immunotherapy, the dual therapeutic effect can be assessed. ^{131}I labeled **4-3** can be injected in mice bearing LNCaP tumours, and tumour growth can be compared to that of a control in which an equal amount of cold **4-3** is injected (immunotherapeutic control). Any increased tumour growth inhibition in mice injected with ^{131}I labelled **4-3** should be a result of the addition of radiotherapy.

4.4 Experimental Section

Cells and Materials: LNCaP cells *(*ATCC no. CRL-1740) were cultured in RPMI 1640 media supplemented with 10% fetal bovine serum, 2 mM L-glutamine, 1 mM sodium pyruvate, 10 mM HEPES, 1% penicillin streptomycin and 0.25% D-glucose. The cell line was cultured at 37 °C and 5% CO_2. RIPA buffer contained 100 mM Tris pH 8, 50 mM NaCl, 1% NP40, 0.5% Na deoxycholate and 0.1% SDS (Bioshop, SDS001.1). TBS consisted of 25 mM Tris-HCl, 150 mM NaCl, 1.5% BSA, 5 mM glucose and 1.5 mM

$MgCl_2$. All chemicals and reagents were purchased from Sigma-Aldrich unless otherwise indicated.

Fluorescence Assay: LNCaP cells were detached from the flask and re-suspended in TBS, having a density of 6.25×10^5 cells/mL. Aliquots of 0.2 mL of the cell solution were prepared in Eppendorf tubes. Four solutions were prepared by adding either 20 μL of 5 μM **4-1**, **4-2**, or **4-3**, along with either 18.4 μL vehicle (non-block) or 22.1 mM PMPA (block), to 400 μL TBS. Additionally, 20 μL of 2 mg/mL AlexaFluor488 conjugated rabbit anti-dinitrophenyl IgG – fraction KLH (Invitrogen) was added to each of the four solutions. 57.3 μL of each solution was added to six Eppendorf tubes each containing the LNCaP cells. Aliquots were incubated at 37 ˚C for 1 hour on a shaker. To each tube, 750 μL TBS was added, and the cells were washed an additional time with TBS. PBS was used to wash the cells once more. Three of the six aliquots in each group were re-suspended in 0.5 mL PBS and 2 μL of 500 μg/mL propidium iodide was added to these samples, and the cells were analyzed with the BD LSR II Flow Cytometer. The remaining set of aliquots were re-suspended in 0.5 mL lysing buffer and incubated at 37˚C. Three 150 μL aliquots of each 500 μL lysed cell sample was added to a 96-well plate, and fluorescence intensity was analyzed with the Tecan Infinite M1000 plate reader by exciting at 494 nm and reading the fluorescence intensity at 520 nm.

4.5 References

1 Murelli, R. P., Zhang, A. X., Michel, J., Jorgensen, W. L. & Spiegel, D. A. Chemical control over immune recognition: a class of antibody-recruiting small molecules that target prostate cancer. *J Am Chem Soc* **131**, 17090-17092 (2009).

2 Vallabhajosula, S., Smith-Jones, P. M., Navarro, V., Goldsmith, S. J. & Bander, N. H. Radioimmunotherapy of prostate cancer in human xenografts using monoclonal antibodies specific to prostate specific membrane antigen (PSMA): studies in nude mice. *Prostate* **58**, 145-155 (2004).

3 Shawn Hillier, K. R., Kevin Maresca, John Marquis, Mathias Tesson, Craig Zimmerman, William Eckelman, Rob Mairs, John Joyal and John Babich. [131I]MIP-1466, a small molecule prostate-specific membrane antigen (PSMA) inhibitor for targeted radiotherapy of prostate cancer (PCa). *J Nucl Med* **53**, 170 (2012).

4 Dubrovska, A. *et al.* A chemically induced vaccine strategy for prostate cancer. *ACS Chem Biol* **6**, 1223-1231 (2011).

Chapter 5: Conclusions and Future Work

A series of constructs were evaluated as multi-purpose imaging probes and therapeutic agents. These constructs combined optical and nuclear probes derived from Tc/Re (Chapter 2), PDT and optical (Chapter 3) and immunotherapy/radioiodine based agents (Chapter 4). The photophysical and biological properties of these potential optical/nuclear imaging agents/therapeutics were assessed in vitro.

An isostructural construct that is an optical probe when complexed to rhenium (or by itself) and a nuclear probe when complexed to ^{99m}Tc was assessed first. The optical properties of SAACIII were determined and the peak fluorescence emission was deemed too short for use as an optical probe. The isostructural [2+1] ligands were developed in place of SAACIII, and the rhenium analogues were found to possess a peak emission of around 580 nm. The uptake in MCF-7 cells of two of these derivatives in particular was studied: a pyridine methanol derivative (**2-6a**) and a cyclohexyl nicotinate derivative (**2-7a**).

Radioactive cell assays of **2-6a** and **2-7a** showed constant uptake to 120 min., with **2-6a** having approximately 7% and **2-7a** having approximately 5% uptake at 120 min. Confocal microscopy was performed to evaluate the uptake of the rhenium bipyridine derivatives in MCF-7 cells. Fluorescence of **2-7a**, but not **2-6a**, was observed in MCF-7 cells incubated with 100 μg/mL of the compound for 1.5 h at room temperature. A colocalization study was conducted with **2-7a** and MitoTracker Deep Red. Although

overlap was seen in the images, Pearson's coefficient indicated no colocalization. It is concluded that although **2-7a** may be localizing to the mitochondria, the compound may be present elsewhere in the cell, which would result in a low value for Pearson's coefficient. Notwithstanding the specificity of this particular construct, the results clearly indicate the [2+1] compounds can be used to create new isostructural nuclear and optical probes. By utilizing the fact that mitochondria have an increased mitochondrial membrane potential in comparison to normal epithelial cells, **2-7** has the potential to be a isostructural imaging probe for targeting cancer. Other targeting vectors could also be attached to **2-7** in order to target a specific receptor overexpressed in cancer.

The [2+1] isostructural ligands can be adapted to behave as activatable optical probes that remain optically silent until binding to the target of interest. Our work showed that a [2+1] construct linked to DNP reduced fluorescence intensity by approximately 50%. By attaching the [2+1] complex to tetrazine, the fluorescence could be quenched to an even greater extent. Rossin *et al.* have demonstrated in vivo targeting of a probe containing tetrazine through the cycloaddition of tetrazine and trans-cyclooctene (TCO). TCO was attached to CC49 mAb in order to target tumour-associated glycoprotein 72 (TAG-72). The TCO conjugated CC49 mAb was injected in mice one day prior to the injection of an ^{111}In-labeled probe containing tetrazine. Upon injection in mice, the tetrazine bound to TCO and the probe was therefore directed to the tumour.[1] This targeting method can be adapted for the [2+1] ligands in order to create an optical "smart" probe. Upon conjugation to tetrazine the fluorescence of the [2+1] ligand should be quenched, and upon subsequent binding to TCO, the fluorescence will be restored.[2]

Another [2+1] ligand targeting bone has been developed by the Valliant laboratory. This Re/^{99m}Tc bipyridine ligand contains zoledronic acid, a bisphosphonate, as the monodentate ligand and has been shown to have uptake in bone in SPECT/CT images. Fluorescence images of uptake in osteoclasts are to be obtained using the rhenium analogue in order to demonstrate the dual nuclear/optical imaging ability of this potential probe. Bisphosphonates bind Ca^{2+} ions and will therefore bind bone mineral. Upon bone resorption the bisphosphonates are released and are available to be internalized by osteoclasts. Coxon *et al.* have shown uptake in osteoclasts by incubating 100 μM of their fluorescent bisphosphonate analogue for 4 h with osteoclast cells, and visualizing with confocal microscopy. MCF-7 cells were used as a negative control due to their low endocytic activity.[3] This experiment will essentially be repeated using the fluorescent [2+1] zoledronic acid derivative created in the Valliant laboratory.

Chlorin e6 (Ce6) was also evaluated as a possible targeted photosensitizer and nuclear/optical imaging probe. A set of PSMA-targeted Ce6 constructs were evaluated for binding to the target, and for uptake in a PSMA-positive cell line (LNCaP cells) and a PSMA-negative cell line (PC3 cells). **3-3**, **3-4** and **3-5** were found to have sufficient binding affinity for PSMA, demonstrated using fluorescence microscopy, flow cytometry and a plate reader assay. Fluorescence microscopy and the plate reader assay showed greater uptake of the PSMA-targeted Ce6 compounds in LNCaP cells versus PC3 cells. The plate reader assay showed that **3-3** had the greatest difference in uptake between the PSMA-positive and PSMA-negative cell line, indicating that this construct may be best for targeted photodynamic therapy in order to minimize damage to healthy cells.

In regards to these PSMA-targeted Ce6 constructs, in vitro PDT cell viability experiments should be performed now that the lead compound has been identified. Because there is preferential uptake in PSMA-positive cells versus PSMA-negative cells, there should be an increased therapeutic and cell killing effect in the PSMA-positive cells when PDT is induced. This can be shown in vitro by incubating LNCaP and PC3 cells with the PSMA-targeted Ce6 derivatives for some time, and then subsequently applying laser light of around 670 nm. An MTS or MTT assay can then be used to measure cell viability.

Na and coworkers have performed in vitro PDT experiments with their acetylated-chondroitin sulfate/Chlorin e6 (Ac-CS/Ce6) conjugates in HeLa cells. Concentrations ranging from 0 to 2 μg/mL of their compound, as well as free Ce6, were incubated with HeLa cells for 1 or 6 h, after which the cells were irradiated with a 670 nm laser for 2 min. Cell viability was assessed with a MTT assay, and cell death was found to increase with concentration and incubation time. The Ac-CS/Ce6 conjugate also had slightly more cell death in comparison to free Ce6.[4]

Lastly, a set of antibody-recruiting small molecules containing iodine were evaluated. These constructs can be labeled with ^{123}I and act as a SPECT agent, or be labeled with ^{131}I in order to be a dual-therapeutic agent. Binding to the target (PSMA) and the subsequent recruitment of fluorescently labeled antibodies to the site were evaluated. Specificity was confirmed using a PSMA block (PMPA). Flow cytometry and the plate reader were used to measure the fluorescence intensity due to antibody binding. Compound **4-3** showed the greatest level of antibody recruitment when no block was added. Fluorescence

intensity levels measured were slightly greater than that for **4-1**. When a block was added fluorescence intensity/antibody recruitment dropped greatly for **4-1** and **4-3**. Compound **4-2** was shown to have the greatest binding affinity to PSMA, however, this compound was not able to bind antibodies sufficiently.

The next step for the antibody recruiting small molecules is to perform a maximum tolerated dose (MTD) study and radiotherapeutic study. After determining the MTD using the ^{131}I labeled compound, the determined maximum tolerated dose would be used for further radiotherapeutic studies. The radiotherapeutic effect as a measure of tumour size/growth caused by this dose should be evaluated in a larger group of mice. The immunotherapeutic effect would next be assessed by repeating the studies using **4-3** with cold iodine. The compound would be injected in mice bearing LNCaP tumours and the associated tumour growth inhibition evaluated. Once this is done, a combined treatment would be explored whereby ^{131}I labelled **4-3** is injected in mice bearing LNCaP tumours. The tumour growth would then be compared to that of a control in which only immunotherapy is induced by the injection of cold **4-3**.

5.1 References

1 Rossin, R. *et al.* Highly Reactive trans-Cyclooctene Tags with Improved Stability for Diels–Alder Chemistry in Living Systems. *Bioconjug Chem.* **24**, 1210-1217 (2013).

2 Devaraj, N. K. & Weissleder, R. Biomedical Applications of Tetrazine Cycloadditions. *Acc Chem Res.* **44**, 816-827 (2011).

3 Coxon, F. P., Thompson, K., Roelofs, A. J., Ebetino, F. H. & Rogers, M. J. Visualizing mineral binding and uptake of bisphosphonate by osteoclasts and non-resorbing cells. *Bone* **42**, 848-860 (2008).

4 Li, F. & Na, K. Self-assembled chlorin e6 conjugated chondroitin sulfate nanodrug for photodynamic therapy. *Biomacromolecules* **12**, 1724-1730 (2011).